BENDING STRESSES IN PARALLEL STRAND STAY CABLES

by

Qian Lin

A Dissertation Submitted in

Partial Fulfillment of the

Requirements for the Degree of

Doctor of Philosophy

in Engineering

at

The University of Wisconsin-Milwaukee

May 2023

ABSTRACT

BENDING STRESSES IN PARALLEL STRAND STAY CABLES

by

Qian Lin

The University of Wisconsin-Milwaukee, 2023
Under the Supervision of Professor Habib Tabatabai

Stay cables are the most important structural elements that support a cable-stayed bridge span. Although stay cables are primarily tension elements, they are also subjected to bending stresses due to the application of transverse loads on the cable, end rotations due to the deck and tower movements, and cable vibrations. Due to their potential impact on fatigue, bending stresses are an important design consideration for stay cables. Most modern stay cables are composed of parallel 7-wire greased-and-sheathed strands that are bundled together. The individual 7-wire strands are splayed out near the anchor heads at the ends of the cable, and each strand is terminated at a specially designed wedge-socket system at the anchorage plate. Traditionally, designers have assumed that the strands form a non-composite bundle due to a lack of sufficient bond between strands along the length of the cable. This assumption ignores the fact that relative slippage between strands (needed for full non-composite action) cannot occur at the anchorage (i.e., compatibility of deformations is enforced at the cable ends even though the strands are not in contact with each other in the transition zone). The governing design standard for parallel strand stay cables in the U.S. (PTI DC-45), as well as industry practice, considers the apparent angular rotation as the only parameter influencing bending stresses in stay cables, while the influence of cable size and length is not considered. In this study, the development of bending stresses in stay cables is examined through experimental

and computational models. Simplified calculation procedures for bending stresses are proposed. The computational models and the proposed calculation procedures are verified using laboratory experiments performed on single-and 5-strand cables. The bending-induced stress generated in each strand is proportional to the average eccentricity of that strand from the centroid of the cable within the transition zone (between anchorage and tension ring). Bending stress is also proportional to the rotation angle within the transition zone (θ) and is inversely proportional to the cable length (L). Furthermore, there is an axial stress increment due to the elongation of the cable under load. Therefore, the commonly made assumption that rotation angle alone can represent the bending stresses in a stay cable is not valid. Bending stresses for a given angle change can be substantially higher in shorter cables with many strands.

Dedication

I dedicate this dissertation to my dear wife, son, my parents, brother, and my parents-in-law, who have given me endless courage and strength, as well as a beautiful life I love.

TABLE OF CONTENTS

LIST OF FIGURES

LIST OF TABLES

ACKNOWLEDGEMENTS

I would like to express my sincerest appreciation to all those who have supported me during my doctoral research.

First of all, the holy grail goes to my advisor, Dr. Habib Tabatabai. This dissertation was completed under his extremely careful and patient guidance. His rigorous academic requirements, meticulous guidance, superb wisdom, broad knowledge, and at critical moments, his ability to overcome difficulties allows my research project to be completed smoothly. Moreover, his amiable attitude towards people and his harmonious and cooperative style have benefited me a lot.

I would like to sincerely thank my family for their selfless support and for taking care of my wife and son so that I can successfully complete my wonderful Ph. D. journey.

I offer sincere gratitude to my dissertation committee members, Dr. Rani Elhajjar, Dr. Devendra Misra, Dr. Yongjin Sung, and Dr. Hua Liu, for their constructive feedback, insightful comments, and kind guidance, which have greatly improved my dissertation.

It is also a great pleasure to thank Dr. Rani Elhajjar for his support in my experiment. Many thanks to the UWM Structural Engineering Laboratory, dear Dr. Hua Liu, dear Mr. Rahim Reshadi, Ms. Farzaneh Elyasigorji, Mr. Farhad Farajiani, and Mr. Barbod Mehrbod and the Machine Shop of the College of Engineering and Applied Science, for providing me great help for my experiments.

Chapter 1: Introduction and research backgrounds

1.1. Introduction

Copper cables (made with copper material) were used in structures as early as 700 BC (Costello, 1978). In modern times, cables made of parallel or helical steel wires/strands are widely used in buildings, stadiums, cable-supported pedestrian and highway bridges (Figure 1-1), guyed towers (Figure 1-2a), power transmission networks (Figure 1-2b), etc. Cables are generally considered to primarily resist axial tension based on an idealized assumption of a moment of inertia of zero. However, bending moments and stresses can also be generated in the cable due to applied loads and vibration because of the non-zero bending stiffness (moment of inertia) in real cables.

Stay cables are a particular type of structural cable used as primary support in cable-stayed bridges. Cable-stayed and suspension bridges are both cable-supported structures that incorporate one or more pylons (towers) in which cables support the bridge superstructure. In stay cables, inclined cables are installed between the deck and the pylon(s). Because of their geometric arrangements within the cable-supported structures, stay cables are susceptible to fatigue and bending stresses. This thesis is focused on bending stresses in stay cables. However, prior research on bending stresses in all structural cables is reviewed to inform this research on stay cables.

Figure 1-1. A Cable-stayed Bridge--6th Street Viaduct, Milwaukee, Wisconsin (Photos by Qian Lin)

(a) Guyed tower (b) power transmission networks

Figure 1-2. Helical cables used in electrical applications (Photos by Qian Lin)

At the ends of a typical bridge stay cable, rotations due to deck and tower movements as well as vibrations, wind, or other loads acting on the cable itself can create bending deformations and stresses in a stay cable (Gimsing, 2011) (Figure 1-3a). Similarly, the vertical hanger cables of arch bridges could develop bending stresses under the longitudinal thermal movements of the structure (Figure 1-3b)

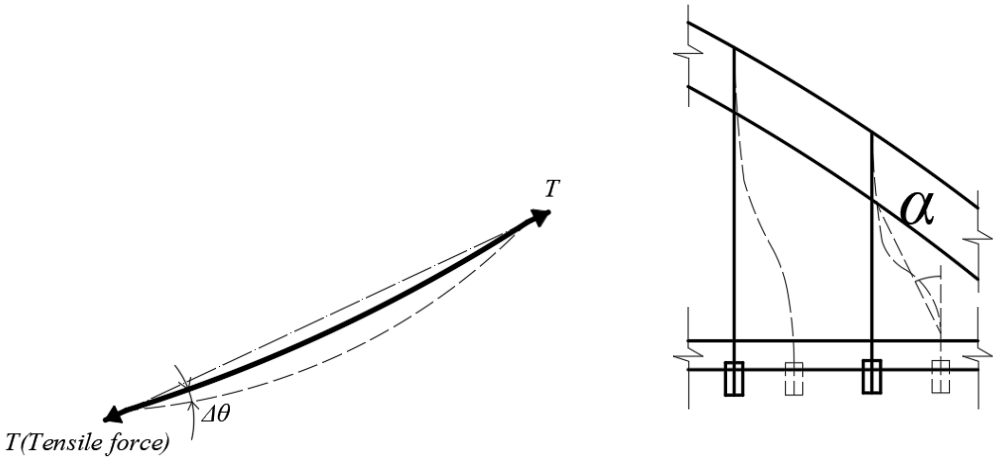

(a) Angular change at a stay cable end under varying sag (Gimsing, 2011) (b) Lateral bending caused by the longitudinal deformation of bridge decks

Figure 1-3. Bending deformation of bridge cables

One contributor to the development of bending stresses in stay cables is the rotation of the deck and towers (at the cable ends) due to the application of various loads on the structure (Figure 1-4a). Moments and stresses developed in the cables due to end rotation depend on cable tension, bending stiffness, and the length of the cable. Loads applied to the cable along its length also generate bending stresses (Figure 1-4b).

The Post-Tensioning Institute (PTI) standard on stay cables (DC-45 2018), the International Federation for Structural Concrete (fib) Bulletin No. 89 (fib 2019), and others have traditionally implied that the bending stress at the anchorage of a stay cable can be represented by the apparent angle change introduced due to loading (Figure 1-4b). PTI DC-45 (2018) specifies that an angle change of 25 milli radians "occurring at the entrance of the stay cable into the anchorage or at any other location in the anchorage where the stay cable may be assumed to be deviated" should be the basis for assessing the bending strength of stay cable at the anchorage.

Designers have traditionally ignored the potential composite action in stay cables between 7-wire strands in a parallel strand bundle except when grouted strands are used. In modern stay cables, the cable is a bundle of greased and individually sheathed 7-wire strands that are splayed out near the anchorages and terminate in anchorage plates (Nabizadeh et al. (2021). The PTI standard (DC-45 2018) states: "For individually protected MTE [main tension element] without grouting of the stay cable, the stiffness may be assumed as the sum of the stiffness of each individual MTE." This suggests that composite or partially composite action should not be assumed, and the cable should be considered to be a set of independent strands when considering bending stresses in cables.

The same approach is taken for bending qualification tests of stay cable anchorages. The fib Bulletin No. 89 (fib 2019) specifies cable bending test requirements, which are based on imposition of angle changes of ±10 milli radians for 100,000 cycles followed by ±25 mili radians for 2 million cycles. A transverse load is applied at the center of a short-stay cable test specimen to impose the required angle changes (Figure 1-5). The cable length for the test cable can be variable with a minimum length of 3500 mm (11.48 ft). The test cable can have any number of strands. The apparent angle change is determined by dividing the cable deflection under the transverse load by half the length of the cable. This approach implies that angle change is a measure of bending stress regardless of the size of the cable or its length.

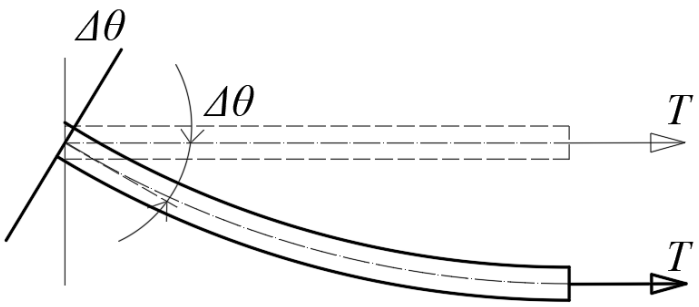

（a）An angular change imposed at cable end

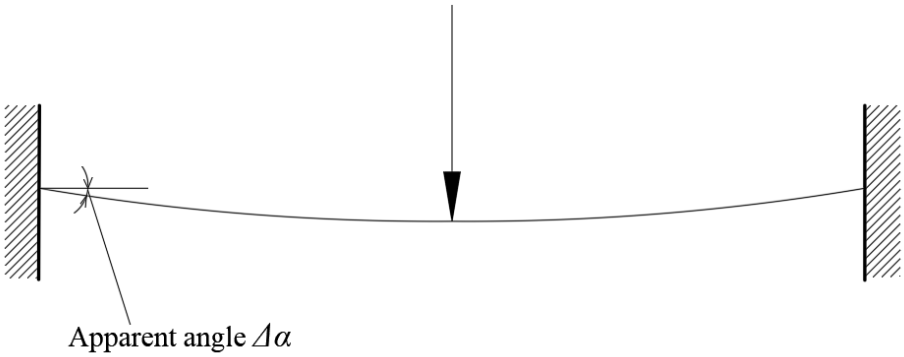

(b) Angular changes caused by transverse load.

Figure 1-4. An angular change at the cable end

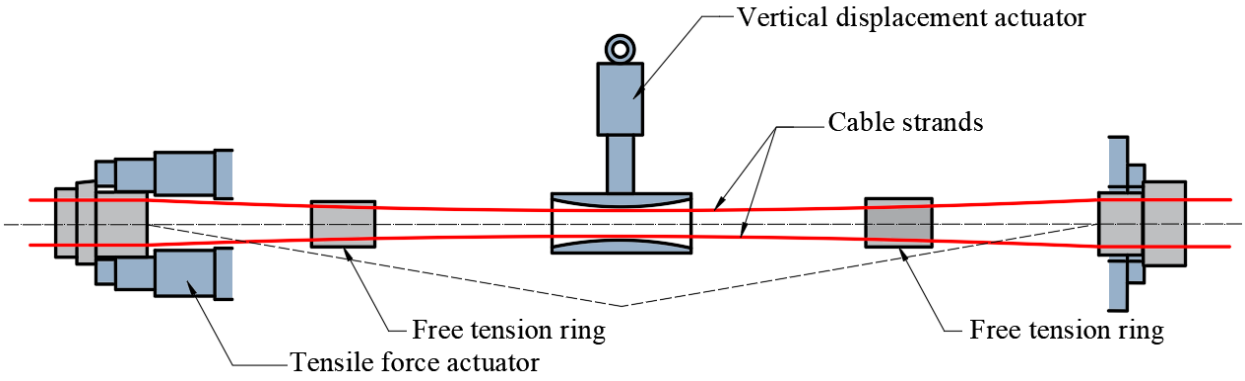

Figure 1-5. Bending fatigue test setup (Adapted from fib 89 (2018))

A Texas Department of Transportation (TxDOT) special specification (Special Specification 4604, 2004) stipulated that the angle change of the strand in the anchorage or transition zones should not exceed 0.025 radians. It is also specified that the bending stress in each strand

should not be larger than 36 ksi in the transition zone at the entrance to the anchorage under an angle change of 0.03 radians.

Based on the classical elastic theory of structural mechanics, the following relationship exists between slope of the deformed (θ), curvature (ψ), and bending moment (M). In linearly elastic beams, the curvature is proportional to the bending moment, and the angle change between two points on the deflected shape is the integral of the curvature equation between those two points, as shown in the following equations. In an elastic beam with perfectly bonded elements, bending stresses are a function of curvature. Angle change between any two points on the deflected shape of a beam (1 and 2) is equal to the integral of curvature diagram between those points.

$$\frac{d_y}{d_x} = \theta \qquad (1\text{-}1)$$

$$\psi = \frac{d_\theta}{d_x} = \frac{M}{EI} \qquad (1\text{-}2)$$

$$\psi = \frac{d^2 y}{d_x{}^2} = \frac{M}{EI} \qquad (1\text{-}3)$$

$$\Delta\theta_{12} = \int_1^2 d\theta = \int_1^2 \frac{Mdx}{EI} \qquad (1\text{-}4)$$

Parameters y, θ, M, ψ, and EI are displacement of the beam at position x along its length, θ is the slope of the deflected curve, M is the bending moment, ψ is curvature, and EI is flexural rigidity. Considering that each strand in a multi-strand stay cable terminates at a rigid anchorage plate, and the connection is not a hinged connection, the angle change cannot occur right at the anchorage. Instead, angle change occurs over a distance (typically within the transition zone). Transition zone is the area near the anchorages where strands are slayed out (separated) from the bundle, with each strand individually anchored at the anchor plate. Within

the transition zone, the strands are fully separated from each other, but they are still constrained at the two ends of the transition length (anchorage and the tension ring). Relative slippage between strands cannot occur at the anchorage plate, and the strands bend individually within the transition zone. While using angle change as a measure of bending stress is simple and convenient for designers, its accuracy must be evaluated since bending stress is also a function of cable size and cable length. The consideration of angle change as a single measure of bending stress would imply that short, long, small, and large cables would all result in the same bending stress if the imposed angle change were the same (Figure 1-7).

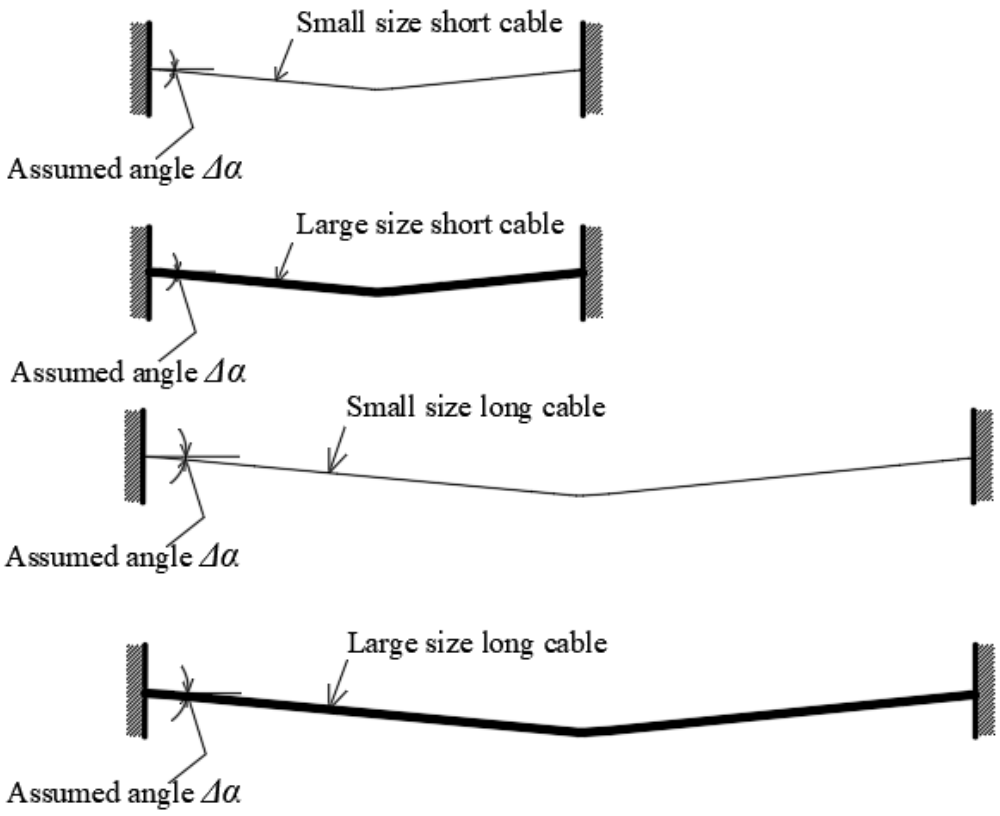

Figure 1-7. Angular changes caused by midspan deflection with different cable sizes and lengths.

In the calculation of the moment of inertia (I), the standards and many practitioners assume that composite or partially composite action does not exist anywhere along the stay

cable, whether in the transition zone or in the free length of the cable. Rather, the cable's moment of inertia is considered to be equal to the number of strands in the cable (n) times the moment of inertia of a single strand (I_s)

.

$$I_{nc} = n \times I_s \quad (1\text{-}5)$$

$$I_c = n\, I_s + \sum A_s \cdot D^2 \quad (1\text{-}6)$$

Where, I_c and I_{nc} are the composite and non-composite moments of inertia of the cable, respectively, n is the number of strands, I_s is the moment of inertia of a single strand, A_s is the cross-sectional area of a single strand, and D is the vertical distance between the centroid of a strand and the center of the cable (Figure 1-8).

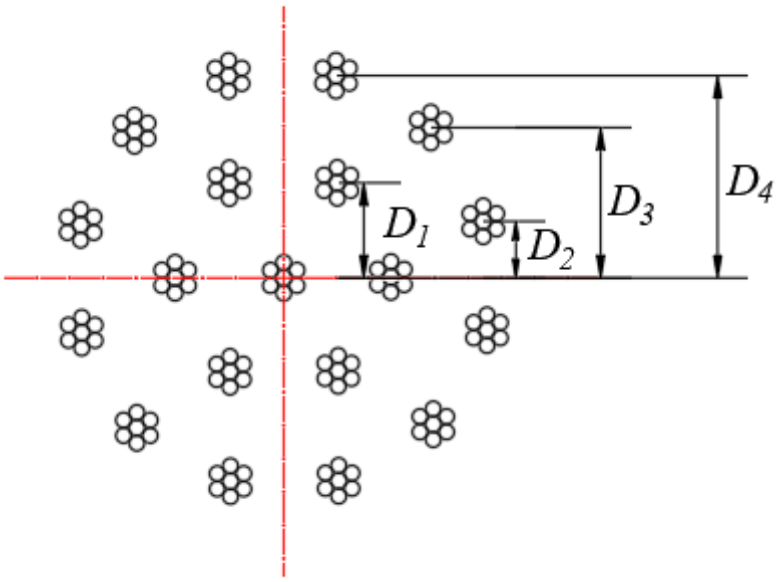

Figure 1-8. Cross section of a 19-strand stay cable at the cable anchorage.

Figure 1-9(a) shows the longitudinal cross-section of a typical stay cable near the anchorage. All strands terminate at wedges in the anchor head. For non-composite action relative slip of strands would be expected to occur due to bending action. In the anchorage setup for stay cables, no relative slip can occur between the strands, and the anchor head imposes compatibility at the cable ends even though the strands are fully non-composite (without contact) within the transition zone. If the strands were fully non-composite, then all strands should experience the same stress if a transverse load was applied to the cable. This study aims to understand the bending stress response of a bundle of 7-wire parallel strands in typical stay cables and propose computational approaches to calculate bending stresses due to transverse loads applied on the cable.

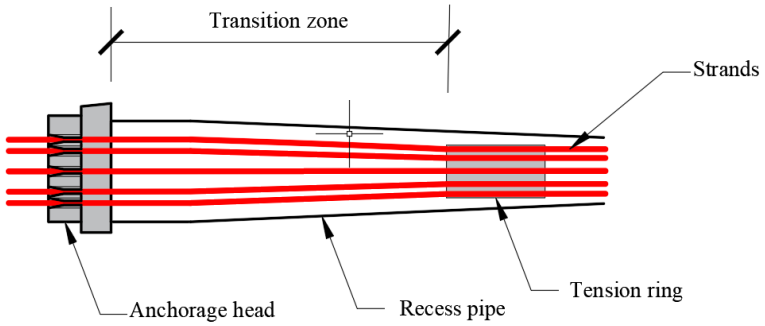

(a) Longitudinal cross section of a stay cable near the anchorage area.

(b) 7-wire strand anchorage.

Figure 1-9. Stay cable anchorage.

Considering that the anchor heads, where all cable strands terminate, do not allow relative slip between individual strands (i.e., compatibility is enforced at the anchorage) and considering that a strand bundle is typically banded together at intervals along the free length of cable using cable bands, the assumption of non-composite action or the degree of any composite action should be evaluated. The bending stiffness of the stay cable at various locations along the length of the cable should be compatible with the extent of composite action between individual strands. Within the transition zone, there is no contact/compatibility between the strands as they are free from each other. However, at the two ends of the transition, the strands are constrained by the anchorage plate and the tension ring. This is analogous unbonded post-tensioning tendons in beams where eccentricity of the tendon matters even when there is no strain compatibility between the tendon(s) and the rest of the concrete section between anchorages and/or deviation blocks.

This work explores the bending stresses in stay cables composed of parallel 7-wire strands due to transverse loads. The factors affecting bending stresses in stay cables is examined through experimental testing and computational models (finite element and finite difference).

1.2. Research Significance

Bending stresses are important considerations in fatigue resistance of stay cables in cable-stayed bridges. This research tests the validity of the traditional approach used by designers to consider angle change as a sole measure of bending stress in stay cables and proposes simplified equations for calculating bending stresses.

1.3. Objectives

The primary objectives of this research are:

- Determine the extent to which composite section can be achieved between strands in a 7-wire parallel strand stay cable, especially near the anchorage zones.
- Determine whether the commonly used angle change is a valid single measure of bending stresses in stay cables subjected to transverse loading along their length. Identify other influential factors that may affect bending stresses in cables.
- Propose simplified relationships to determine bending stresses in parallel 7-wire strand stay cables under the action of transverse loads. Conduct parametric studies to illustrate the influence of various parameters on bending stresses.

1.3. Scope

In this thesis, the factors affecting bending stresses in stay cables are examined through experimental testing and computational modeling. In the experimental program, two tests involving a single strand and a 5- strand cable were first performed (based on the fib Bulletin 89 bending test setup) to measure the tensile and bending forces and strains in strands (as measured with strand load cells and strain gages), and to assess the influence of multiple strand cable on strand forces. Angle changes of up to 25 milli radians were statically imposed. A comparison of the two tests would indicate the effect and degree of composite action between strands. Without any composite action, the forces in individual strands of the 5-strand cables would theoretically be the same as the force in the single-strand cable. Secondly, the single strand and 5-strand cable tests are simulated using finite element models under axial tension

and imposed mid-span displacements. The variation of axial and bending stresses and strains in the single strand tests is studied though finite element modeling of all seven wires in each strand (the straight king wire and spiral outer wires) as well as friction between wires and between wires and the strand sheathing. The experimental work is used to verify and calibrate computational models. An equivalent (simplified) cylindrical model of the 7-wire strand is proposed. The simplified model would substantially reduce the computational cost (time) of performing finite element model of parallel strand cables. The finite difference approach proposed by Mehrabi and Tabatabai (1998) is also used to verify the results of finite element models and the experiments, and to allow a more rapid analysis and determination of angle changes for any cable size and length. Based on the results of experimental and computational models, a simplified equation is proposed to estimate bending stresses in stay cables subjected to transverse loading. This research provides an answer as to whether the long-standing use of angle change as a measure of bending stress in cables is a valid approach.

1.4. References for Chapter 1

Costello, G. A. 1978. Analytical investigation of wire rope. Appl. Mech. Rev., 31(7), 897–900. https://doi.org/10.1061/JMCEA3.0002807.

FIB Bulletins 89, 2019. Acceptance of stay cable systems using prestressing steels. The International Federation for Structural Concrete (FIB). https://www.fib-international.org/publications/fib-bulletins/acceptance-of-stay-cable-systems-using-prestressing-steels-pdf-detail.html.

Gimsing, N.J. and Georgakis, C.T., 2011. Cable supported bridges: Concept and design. John Wiley & Sons.

Mehrabi, A.B. and Tabatabai, H., 1998. Unified finite difference formulation for free vibration of cables. Journal of Structural Engineering, 124(11), pp.1313-1322. https://doi.org/10.1061/(ASCE)0733-9445(1998)124:11(1313).

Nabizadeh, A., Al-Barqawi, M.O. and Tabatabai, H., 2021. Probabilistic Models for Fatigue Resistance of Seven-Wire Prestressing Strands and Stay Cables. Journal of Bridge Engineering, 26(10). https://doi.org/10.1061/(ASCE)BE.1943-5592.0001768.

PTI DC-45, 2018. Recommendations for Stay Cable Design, Testing, and Installation (DC45.1-18), written by PTI Committee DC-45: Cable Stayed Bridge.

SPECIAL SPECIFICATION, 4604 Stay Cables, 2004, Texas Department of Transportation (TxDOT). https://ftp.dot.state.tx.us/pub/txdot-info/cmd/cserve/specs/2004/spec/ss4604.pdf

Chapter 2: Bending Stresses in a Single 7-Wire Prestressing Strand

2.1. Abstract:

Stay cables are critical structural elements in cable-stayed bridges. Due to their potential impact on fatigue resistance, bending stresses are an important design consideration for stay cables. Modern stay cables are typically composed of parallel 7-wire greased-and-sheathed strands that are bundled together. Each strand is terminated at wedges in an anchor head. Studying the bending properties of bundled cable-stayed members requires knowledge of the bending behavior of a single strand. The bending stresses in a 7-wire strand (0.62 in diameter greased-and-sheathed) are investigated under the application of a transverse load at its mid-length. Finite element (FE) and finite difference (FD) models were developed and compared with experimental results. The FE models consisted of the center wire and six outer wires including wedges and other anchorage hardware. An equivalent (simplified) cylindrical model with special boundary conditions was also proposed to properly represent the strand behavior. Both FE models and the FD model were in good agreement with the experimental results. The variations of bending moment at the end regions of the strand can be properly represented in the simplified model using boundary conditions that partially constrained the end surfaces of the cylindrical model. The bending stiffness of the individual 7-wire strand can be assumed to be the composite moment of inertia of the strand wires.

Keywords: Stay Cables; 7-Wire Strand; Bending Stress; Finite Element Analysis; Finite Difference Method.

2.2. Introduction

Seven-wire strands are the primary components of parallel strand stay cables used in modern cable-stayed bridges worldwide. Bending stresses in stay cables are important design considerations, especially with respect to fatigue. To better understand the bending behavior of parallel strand cables, it is important to first understand the bending behavior of the single strand. The modern stay cables consist of 7-wire greased-and-sheathed strands with a polyethylene coating on each individual strand (Nabizadeh et al. 2021). In the US, the strands must meet the design and quality control requirements of the Post-Tensioning Institute (PTI) DC-45 standard (PTI DC-45 2018) to be used in stay cables.

Although the bending behavior of helical strands has been studied, especially in the context of power transmission line cables, there is little prior research of bending stresses in 7-wire strands in the context of modern stay cables. This work addresses the behavior of single-strand greased-and-sheathed7-wire strands as a first step in understanding the bending behavior of parallel strand stay cables. In a single strand cable subjected to bending stresses, studies have shown that wires may slip with respect to each other and contact friction between the wires plays an important role (Papailiou, 1995). The bending stiffness differs between the non-slip stage (where no slip occurs between wires) and after slippage (where wires still interact with each other through friction). In the bending process, as the curvature increases, the unbalanced force between the wires will increase. However, as long as this force is smaller than the friction force between the contact surfaces, there will be no slip. In the non-slip stage, the strand section can be regarded as a solid rod with linear response to bending moments. When the

unbalanced force generated by bending the wires exceeds the friction resistance between wires, interwire slippage occurs, and the bending response of the structure becomes non-linear (Khan, 2018).

Due to the special structure of the helical wires and the potential slippage between wires, the strand stiffness may not be uniformly distributed during loading. To accurately determine the bending stress in a single strand cable, it is important to study the variation of its stiffness along the length of the cable. This can then lay the foundation for determining the bending stiffness of the bundled multi-strand cables.

Several studies have focused on analyzing the bending behavior of single strand stay cables. After applying an axial tension to a pheasant conductor (an overhead electrical conductor cable used in power transmission), Scanlan et al. (1968) measured the deflections of 15 points along a vibrating cable specimen. They calculated the slope and curvature by calculating the first and second derivatives of the deflected shape. Then the bending stiffness was determined. The authors reported that stiffness was not constant along the cable span. It was higher near the end clamps but decreased along the span. A model proposed by Raoof et al. (1984) considered the layers of wires in one strand as orthotropic cylinders, which were used to calculate the bending stiffness. Constant bending stiffness was used in the analysis, and when calculating the weighted layer stiffness, the effective elastic modulus was considered as one of two extreme cases, no slip and full slip. Lanteigne (1985) derived a stiffness matrix for aluminum conductor steel reinforced (ACSR) electrical conductor cables under static tension, torsion, and bending. It was reported that, with an increase in curvature, the outer layer of steel wires could slip by overcoming friction, resulting in a reduction in bending stiffness. The

tension level affects the bending stiffness of the strand, and slip occurs when the interlayer friction is greater than the friction coefficient multiplied by the radial force between wire layers.

LeClair and Costello (1988) proposed a model for calculating stresses on a single strand under axial, bending, and torsional action in the presence of friction. Six nonlinear equilibrium equations were established to calculate the loads required to maintain equilibrium. The tensile stresses generated by bending in the outer wires were determined considering the curvature and twist.

Raoof (1990) studied the response of helical strands to bending moment and axial force. In the critical areas near the terminations, a theoretical stiffness equation describing the slippage between strand layers was derived. The results also confirmed a phenomenon observed in previous bending-fatigue experiments in which the first wire would fail at the neutral axis of the bending, rather than at the extreme fiber position.

Goudreau et al. (1993) conducted flexural tests on an epoxy-coated (49 mm diameter) 7-wire strand. In addition to tensile force, a transverse load was applied at the middle of the cable. The apparent bending stiffness increased with an increase in axial force. This change was affected by the types of boundary conditions, the magnitude of the transverse load, and the variation of the bending moment along the strand. The influence of a slippage coefficient was considered in the bending equation as represented by the ratio of the maximum and minimum stiffness values and based on boundary conditions and lateral loads. The minimum stiffness is the sum of the stiffnesses of single wires, and the maximum stiffness is equal to the minimum stiffness plus the distance effect due to parallel axis theorem as follows:

$$I_{min} = n\frac{\pi d_w^4}{64} + \frac{\pi d_c^4}{64} \quad (2\text{-}1)$$

$$I_{max} = I_{min} + \frac{n}{2}\frac{\pi d_w^2}{4} r^2 \quad (2\text{-}2)$$

Where, d_w is the diameter of the wire diameter, d_c is the diameter of the core wire, r is the radius of the outer wire layer $r = \frac{d_w + d_c}{2}$, and n is the number of wires in the outer layer. The slippage coefficient was defined as follows:

$$K = \frac{EI - EI_{min}}{EI_{max} - EI_{min}} \times 100 \quad (2\text{-}3)$$

Where E is the modlus of elasticity and I is the apparent moment of inertia. K was obtained from bending tests. In bending case with simply support, K varied from 30% (Fz=4. 5kN) to 65% (6.5kN<Fz<11kN), in the fixed support case, K went from 25% (Fz=4.5kN) to 30% (Fz=11kN), Fz is the axial force.

Huang et al. (1994) established a six- wire cable model for uniform bending that considered friction and slip between wires. It was found that there was a critical bending curvature that would cause slip between wires, with the slip starting at the neutral axis and then spreading symmetrically across the entire cross-section. When slippage occurs, bending stiffness changes and the cable may not be regarded as a solid bar. When there is no slip in wires, the bending stiffness of the wires can be considered a solid bar.

Jolicoeur et al. (1996) adopted semicontinuous modeling to study the bending behavior of multilayer wire strands. A layer of wires in a steel strand was considered to be equivalent to a cylinder made of transversely isotropic material, and equations describing the behavior of this orthotropic cylinder were derived under flexural, tensile, and torsional loads. The model allowed the evaluation of strand stiffness, contact stresses, interlayer shear stresses, and slip.

The semicontinuous model obtained accurate results under tensile and torsional loads. However, it was difficult to verify the model under bending.

Hong et al. (2005) established a mesoscale mechanical model for bending characteristics of helically wrapped strands under tensile force, based on an extension of Papailiou's (1997) model and considering the nonlinear behavior of the cable caused by sliding under the action of friction. The results showed that the bending stiffness decreased rapidly with increased cable curvature. From sticking to the fully slip state, the transition depended on the cable tension and friction coefficient. Paradis et al. (2011) extended Papailou's (1997) model by studying the free-bending behavior of multilayer strands and taking into account the tangential compliance of the contact interface. Considering shear, micro-slip, and gross slip at interlayer wire interface, an equation for determining the effective bending stiffness of cable was derived.
Ceballos et al. (2008) proposed a method to use the bending stiffness of a stay cable as a regulating variable in estimating cable forces based on measured vibration frequencies. The results showed that the influence of rotational stiffness at the ends of the stay cable on axial force estimation increased with increased bending stiffness.

Yu et al. (2014) used finite element models to analyze the interfacial mechanisms in seven-wire strands under longitudinal and transverse loads and proposed a partially restrained strand model. The results showed that friction had a minimal effect on axial stiffness and a limited impact on lateral stiffness. The finite element analysis successfully predicted the uneven stress distribution under lateral loading.

In summary, the bending properties of the single strand cable are mainly affected by the magnitude of axial tensile force, frictional coefficient, and slippage state between wires, applied

bending moment (related to the magnitude of curvature), and boundary conditions of the strands. As curvature increases, slippage between the wires can occur, reducing the bending stiffness of the single strand cable from its maximum fully composite value. Some studies have examined the relationship between curvature and friction between wire layers, the influence of slip on bending stress and stiffness.

Research Objectives

The objectives of the research on bending of single strands were as follows:

1) Evaluate the near-anchorage bending stresses in single 7-wire greased-and-sheathed strands that are anchored using wedges (in accordance with common stay cable fabrication processes) under transverse loading conditions.
2) Develop a simplified cylindrical finite element model of the 7-wire strand with appropriate boundary conditions and strand stiffness to properly represent the single strand response in multi-strand cable models.

Research Scope

In the 7-wire strands used in stay cables, the strands are terminated at 2- or 3-piece wedges at the anchorage plates (unlike strands used in other applications where various other fittings may be used). These wedges may not fully engage all exterior wires at the anchorage, and stress in some wires may develop over a distance. This further complicates the effective bending stiffness at the higher-moment areas near the anchorage. To evaluate bending stresses in a single 7-wire prestressing strand commonly used in bridge stay cables, experimental and computational works are performed. The experimental work involved load testing of a 0.62-in 7-wire strand subjected to a transverse load. The experiment was then modeled through

detailed finite element analyses and finite difference models. In the detailed finite element model, all seven wires as well as wedges and other anchorage hardware were modeled. This model was verified with experimental results. A simplified cylindrical model was then developed to reduce the significant computational cost of the full 7-wire model. The validity of the simplified model was verified with experimental results.

2.3. Single strand experiment

2.3.1. Specimen and loading frame

Individual strands used in stay cables typically have a 0.6 or 0.62 in diameter and are individually greased and sheathed with a 1.2-mm-thick high-density polyethylene (HDPE) layer. Seven-wire strands used in cable-stayed bridges must meet specific qualification testing requirements to be used in stay cables ("cable-quality strands") (Nabizadeh et al. 2021). Greased-and-sheathed 0.62-in diameter 7-wire strands from a cable-stayed bridge project were donated to the University of Wisconsin-Milwaukee (UWM) for this research by Structural Technologies Corporation of Columbia, Maryland. The experiments were conducted at the Structural Engineering Laboratory at UWM.

The original cut length of stay cable specimens received was 20 feet. A self-reacting load frame was designed and built to accommodate the axial and transverse forces applied on the strand. The specimen and test setup are shown in Figures 2-1 and 2-2. The dimensions of the strands and information on the loading (reaction) frame are shown in Table 2-1. In the

experimental investigation, the single strand cable was first pre-tensioned, and a transverse load was subsequently applied at the mid-point.

Table 2-1. Dimensions of the 7-wire strand specimen and the loading frame

Parameters	Value
Strand length between bearing plates (ft)	14.7
Strand diameter (in)	0.62
Helical wire diameter (in)	0.204
Core wire diameter (in)	0.212
Cross-sectional area of strands (in^2)	0.232
Sheathing thickness (mm)	1.2
Lay length (pitch of helical wire) (in.)	9
Loading beam type	W8×40
Total thickness of bearing plates (in.)	2
Minimum ultimate tensile strength (MUTS, ksi)	270

The reaction frame consisted of two W8×40 steel members. Two steel angles were welded at one-third points of the two beams to brace the beams. Two 1-inch-thick steel plates were used at each end as bearing plates. The hole patterns in the plate used to install the strands are shown in Figure 1 and Figure 2d. This same reaction frame was later used for a 5-strand test. Therefore, the anchorage plates included five drilled holes to accommodate the strands for a subsequent multi-strand test. Since the 5-strand cable had to include tension rings at the ends of the transition zones, the same steel deviation cylinders were also used in the single strand test with short-length strand fillers placed in the cylinder to position the strand at the center of the cylinder (Figure 1c). The same type of steel cylinder (with strand fillers) was used at the mid-length of the strand to allow the application of transverse load.

As seen in Figures 2-2(c) and (c), a center-hole hydraulic jack was used on the live end of the single strand specimen to apply the initial tensile force. At the mid-span of the specimen, a vertical hydraulic jack and load cell was set to apply a transverse force to the strand specimen. Live and dead-end prestressing chucks with two-piece wedges were used. A center-hole load cell was placed between the dead-end chuck and the bearing plate to record strand force during tensioning and throughout testing. Two strain gages were installed on the strand at a distance of 2 in. from the bearing plate. The strain gages were oriented along the helical wires. Deflections of the strand at the point of application of load and the support were measured using LVDTs (Figure 2-3e, f).

(a) Loading frame

(b) Anchorage Plates

(c) Steel tension ring with strand fillers

(d) Strand fillers

Figure 2-1. Loading frame and strand specimen for single strand test experiment

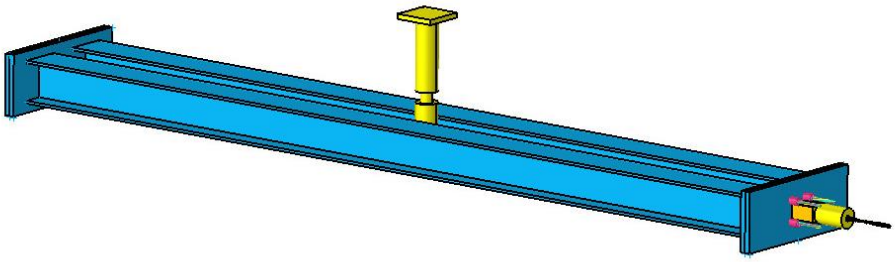

(a) Schematic of reaction frame and loading setup

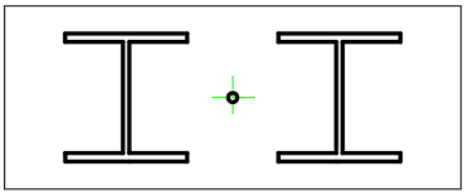

(b) Cross section with single strand. reaction beams and loading plate

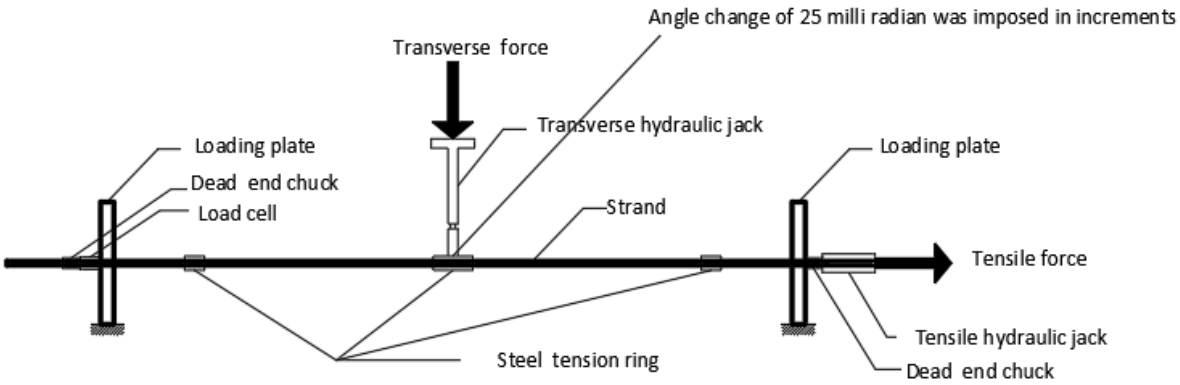

(c)Test setup sketch

Figure 2-2. Loading setup for single strand experiment

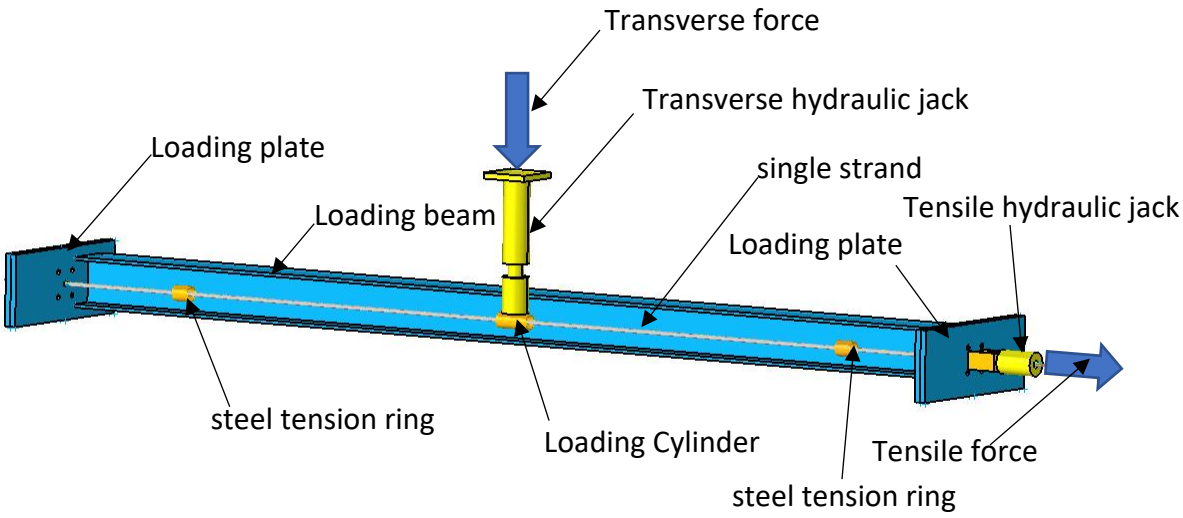

(d)Setup for single strand experiment

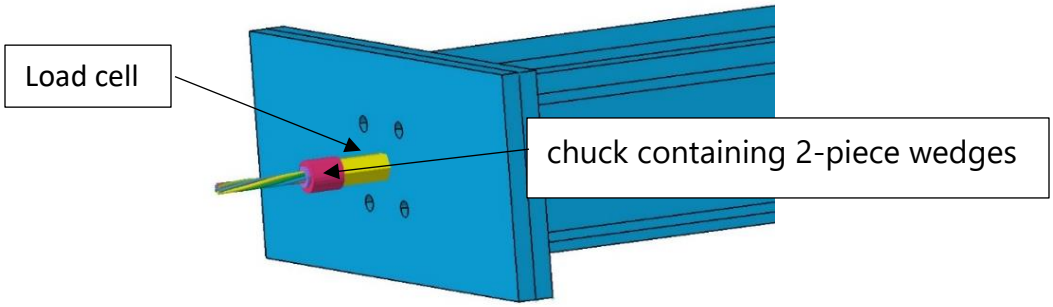

(e) Dead-end chuck and load cell (single strand test)

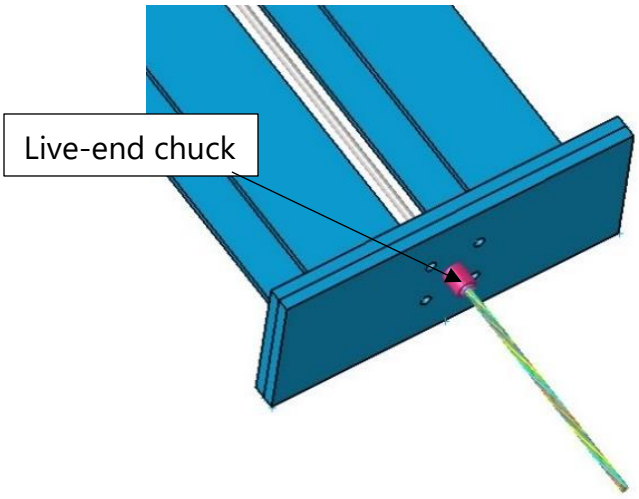

(f) Live end (single strand test)

Figure 2-2. Loading setup for single strand experiment (continue)

2.3.2. Instrumentation and data acquisition.

One LVDT was installed at the mid-length of the strand (near the point of application of transverse load) to measure the mid-span displacement. Another LVDT was placed at the anchorage plate on the dead-end side to measure any downward movement of the steel beam at the support during vertical loading (Figure 2-3 (a) (e), (f)). Two strain gauges were mounted over the top helical wires of the strand two inches from the anchorage plate (Figure 2-3 (g)).

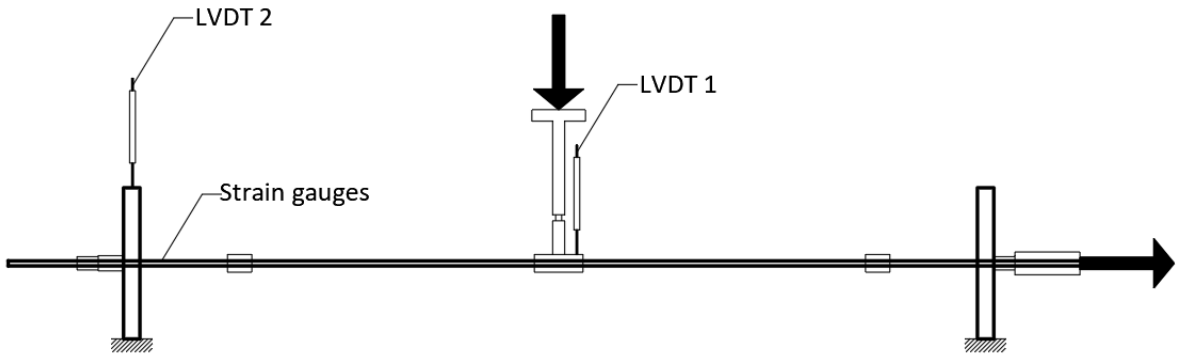

(a) LVDT and strain gauge location

(b) Test setup for single strand experiment

(c) Load cell at the dead end

Figure 2-3. Test setup for single strand specimen

(d) Loading jack at the middle

(e) LVDT at the dead end

(f) LVDT at the middle of the strand

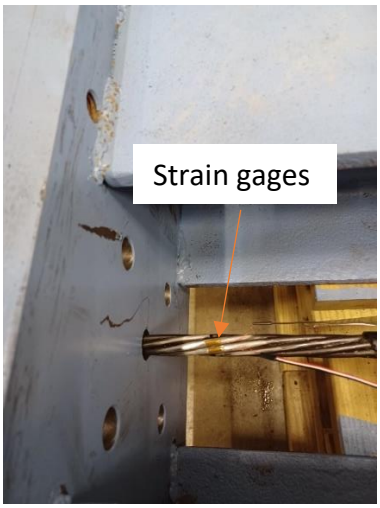

(g) Strain gages' locations on the top two wires of the strand

Figure 2-3. Test setup for single strand specimen (continued)

2.3.3. Loading procedures

A center-hole hydraulic jack and jacking chair were used to apply the tensile force in steps up to a strand load equivalent to 30% of the minimum ultimate tensile strength (MUTS) of the strand ($f_s' = 270\ ksi$). The live-end chuck containing 2-piece wedges was used to seat the

strand. The $0.3f_s'$ tension level was meant to represent the initial dead load stress in the strand before the application of the transverse load.

$$T_s = A_{strand} \times f_s' \times 30\% = 0.232in^2 \times 270ksi \times 0.3 = 18.79kips$$

The strand was then seated on the live end chuck. If the load decreased below the target load due to seating losses, then a jack chair was used to reload the strand and shim behind the live end chuck to increase the tension force to the target value. The load was then transferred to the live end chuck, and the hydraulic jack was removed. A second hydraulic jack was installed at the mid-length of the strand to apply vertical force on the cable to achieve the desired displacement levels at the mid-length of the strand. This loading arrangement is similar to the bending test arrangement specified by fib Bulletin 89 (fib 2019).

The PTI DC-45 standard considers an angular deviation of 0.025 radians as corresponding to the strength limit state for the cable under the application of lateral loads. In accordance with the fib bulletin (reference) described above, mid-length vertical displacements were applied during the bending fatigue tests to represent equivalent angular changes of 0.01 rad (10 milli radians) and 0.025 rad (25 milli radians) at the cable anchorages. For a test cable length of 14.7 ft, the mid-span deflections corresponding to the angular deviation of 0.01 and 0.025 radians would be 0.88 and 2.2 inches, respectively.

2.4. Finite Element Analysis

2.4.1. Model and mesh size

A series of finite element analyses were performed on models of 7-wire strand. The "Hypermesh" and "OptiStruct" modules of the "Altair" commercial software (OptiStruct

Tutorials and Examples) were used for finite element analysis of single strand components. The anchorage system used in the tests (conical chucks with 2-piece wedges) was fully modeled in the analyses to represent the gripping mechanisms based on the conical surfaces of the wedges and the chuck body and considering friction between contact surfaces. The high-density polyethylene sheathing over the strand was also included, except in the end regions where the sheathing was removed in the experiment. All wires were modeled individually with contact between the wires.

For the refined (full) model of the strand, the mesh size of the strand was chosen to be 0.039 in., which is about 1/5 of the wire diameter. Considering the needed calculation time, accuracy, and difficulty of meshing, the mesh size of strands used in this experiment was as follows:

Mesh size: Strand wires—0.039 in (0.001m)

Chucks, load cell---0.059 in (0.0015m)

Bearing Plates, PE cover--- 0.118 in (0.003m)

One-half of the length of the strand was modeled with the appropriate boundary conditions to represent symmetry. The refined FE model for a single 14.7-ft-long strand can be seen in Figure 2-4. The total number of elements was approximately 1,754,000 (including 1,411,500 strand elements). The elements used were 8-point 3-dimensional pyramid solid elements.

(a) Symmetrical model of single strand stay cable

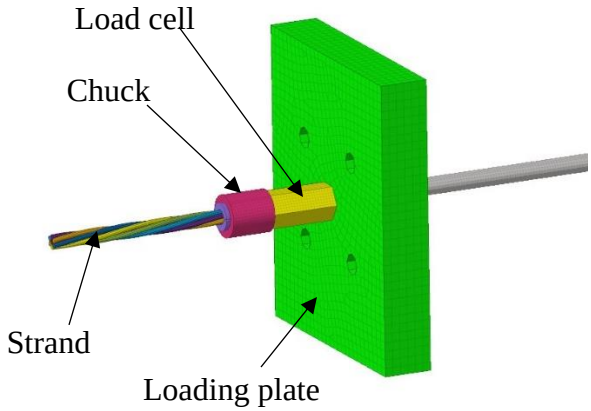

(b) Dead end of the strand

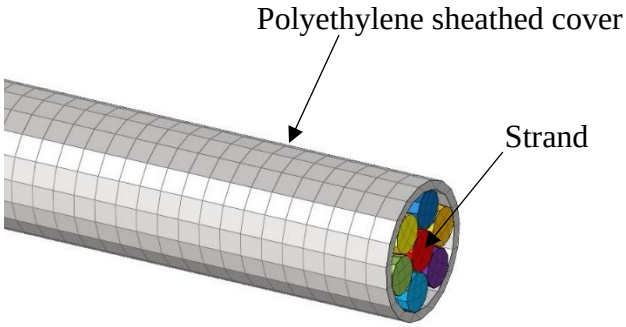

(c) Center cross section

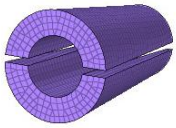

(d) Wedges

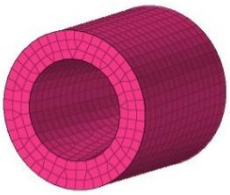

(e) Chuck cylinder

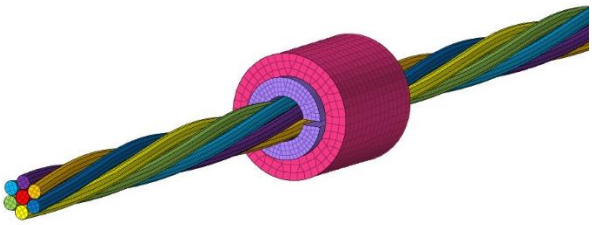

(f) Single strand wires with a chuck

Figure 2-4. Meshes on the FE model of a single strand stay cable.

2.4.2. Contact definition

The contacts defined in the Altair software are static frictional contacts. Since determining the contact areas of helical wires is a very complex issue, the surface-to-surface auto-contact function was used in the Altair-Hypermesh software. To avoid penetration between component surfaces, penalty-based contact was employed.

Judge (2012) proposed that the friction coefficient for wire-to-wire contact was 0.115. Chen (2012) reported that friction between high-strength zinc-coated steel wires was in the range of 0.13 to 0.21 based on experimental results. Considering the presence of grease between wires, a friction factor of 0.1 was chosen. Other friction coefficients chosen were as follows:

(1) Between helical wires and between helical wires and core wire: μ=0.1,

(2) Between helical wires and conical wedges (representing wedge teeth): μ=1.5,

(3) Between conical wedges and the interior surface of the chuck, load cell, loading plates, chucks, and load cell or chucks and loading plates: μ=0.05. These friction coefficients (other than interwire friction) do not have a large effect on the stress results in the strands. These contacts are also defined to avoid penetration. Thus, a small frictional coefficient was selected, thus allowing the slippage of the wedges inside the chuck body as a result of loading.

As the conical 2-piece wedges move inside the cone-shaped surface of the chuck, a transverse force is applied to the wires. And the wedge teeth bite on the surface of the outside wires to grip them. This can be represented by a friction coefficient between the wedges' conical outer surface and the chuck's conical inside surface (Figure 2-5.). Because of the teeth biting the wires, the friction coefficient assumed between these surfaces should be greater than 1.0. In this model, a friction coefficient of 1.5 was adopted, which resulted in a comparable response to the laboratory test results for the single strand.

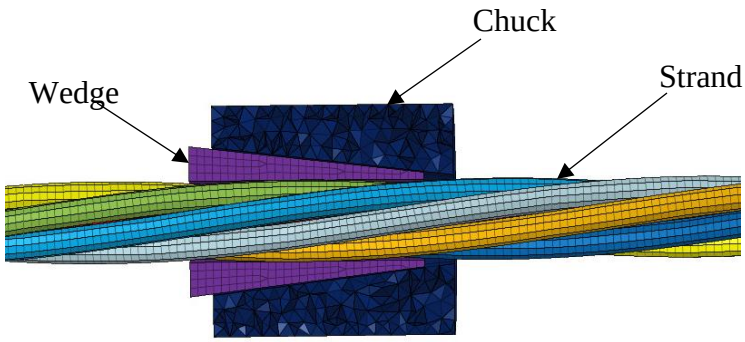

Figure 2-5. Cross section of on the strand with wedges and chuck.

2.4.3. Loading condition

The initial axial stress in the cable (30% of MUTS or 81 Ksi) was simulated by imposing a fictitious cooling temperature change on the wires.

A transverse displacement was imposed in the middle of the single strand cable using the vertical hydraulic jack. The imposed displacements of 0.88 in and 2.2 in correspond to equivalent angular changes of 0.01 and 0.025 radians, respectively.

2.5. Equivalent cylindrical strand model

Since the single strand system comprises seven wires (six helical), the definition of the contact problem becomes relatively complicated, and a substantial computation time is required. To facilitate FE modeling of long cables and multi-strand cables, it is necessary to develop an equivalent representation of the 7-wire strand in the finite element model. Modeling cables with many strands and substantial lengths (i.e., typical stay cables) would lead to a substantial and complicated model with significant difficulties in convergence. It is therefore necessary to develop a simplified (equivalent) FE model that can correctly reflect the deformation and tensile-bending mechanical properties of the 7-wire strand. Accordingly, a

simpler solid cylindrical model of the 7-wire strand is developed. A comparison is then made between the simplified model and the FE model for the full 7-wire strand (0.62 in diameter).

A comparison of the properties of the single strand cable and its equivalent cylindrical model for 0.62-in-diameter strand are shown in Table 2-2. A finite element model of the 0.62 strand with a half-length of 7.35 ft is shown in Figure 2-5. It can be seen from Table 2-2 that, the cross-sectional areas of actual and equivalent strands are the same and their moments of inertia are close while their diameters are different. When calculating bending stress using the equivalent strand model (with smaller diameter), the calculated stress should be adjusted by the ratio of actual diameter of the strand to its equivalent strand diameter. Furthermore, the spiral wires are oriented at an angle α (lay angle) with respect to the axis of the strand. Therefore, to convert bending stresses in the equivalent model to the stresses along the helical wire, a factor of $\frac{1}{\cos \alpha}$ should be applied to the estimated stress (Lanteigne, 1985). The α angle for the strand tested was 12 degrees. Considering these factors, the difference between the bending stress in the equivalent model and the full model would be about 2%. The equivalent model is also symmetrical, and the symmetric boundary conditions can be applied at the mid-span (displacement U1=U3=0, rotation angle R1=R2= 0, U1 is the horizontal displacement, and U3 is the displacement along the cable. R1 and R2 are the rotations about the axes in the plane of symmetry). As shown in Figure 2-6(c).

The boundary condition for the equivalent strand involved pinned connections at the cross section of the cylinder at anchorage. However, the stiffness of this connection must be adjusted such that the developed bending moments near the anchorage do not exceed the experimental results. The wedge anchorage system does not uniformly grab all outer wires at the same level

and there is potential for slippage due to high curvatures. To address this issue, not all nodes in the cross section of the cylinder were provided with pinned connection to control the apparent stiffness. Three vertical nodes at the center of the cylinder were pinned as shown in Figure 2-6b. This is equivalent to 40% of the diameter of the equivalent cylinder or the diameter of the center wire.

Table 2-2 Comparison between actual and equivalent strand properties.

Parameters	Diameter (in)	Cross-sectional area (in^2)	Moment of inertia(in4)
Single 7-wire strand cables			
	0.62	0.232	0.00485
Equivalent cylindrical model	0.544	0.232	0.00429

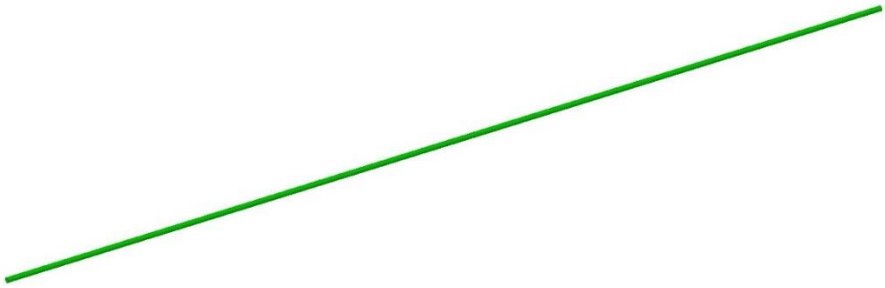

(a) FE equivalent cylindrical model (for the 0.62-in strand)

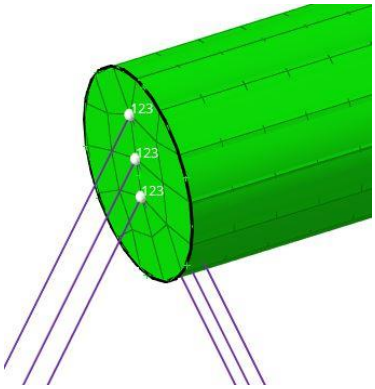

(b) Boundary condition (1)

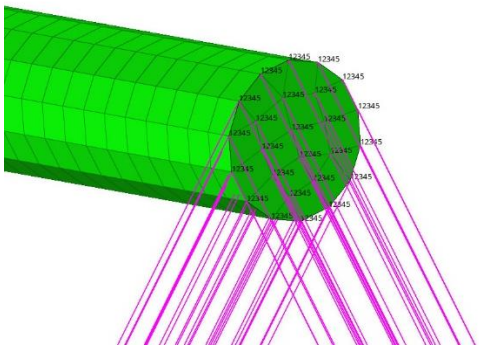

(c) Boundary condition (2)

Figure 2-6. FE the equivalent cylindrical model (for the 0.62-in strand)

2.6. Finite Difference Method

The finite difference (FD) approach for analyzing cables proposed by Mehrabi and Tabatabai (1998) was also used to analyze the single-strand cable and compare with finite element results. The FD approach was developed for assessments of cable vibrations and considers the effect of cable tension and bending stiffness and includes considerations of any intermediate springs and dampers that may be used along the length of the cable. The FD procedures for calculating the static profile of the cable under loads were utilized. The FD procedures can consider both a fixed and pinned end boundary conditions. In this case, the boundary conditions are not fixed or pinned. Therefore, an intermediate boundary condition was selected to conform with the observed experimental results. The FD model was verified using the laboratory test of the 7-wire strand.

The FD approach can be used to quickly analyze the deformation of the cables under the action of various loading conditions and with variable moments of inertia along the length of cable. Firstly, the cables are discretized (Figure 2-7). Then, a stiffness matrix is constructed, which is a function of the modulus of elasticity, tensile force, element size, and the moment of inertia at each node of the discretized cable. A few terms in the stiffness matrix depend on the boundary conditions of either fixed or pinned. However, those values can be adjusted for intermediate levels of fixity at boundary conditions.

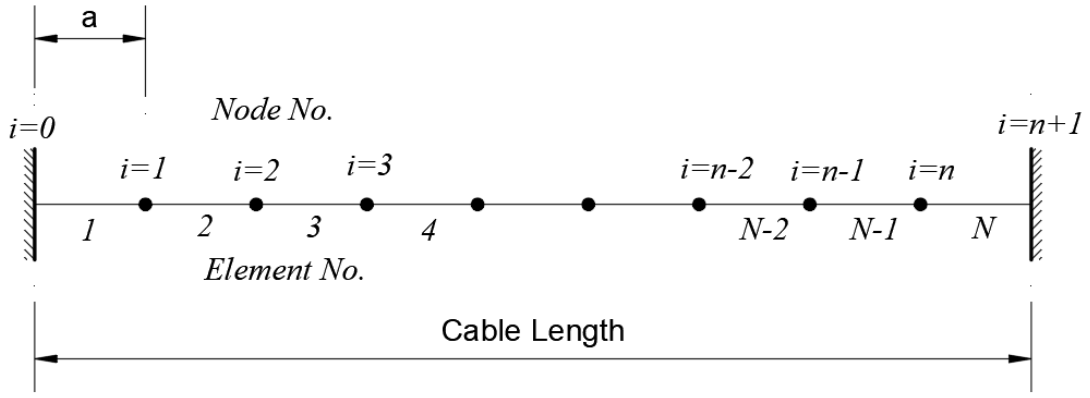

Figure 2-7. Cable discretization for FD modeling (Mehrabi and Tabatabai 1998)

The relationship between the vector of nodal forces (F) and the vector of nodal displacements (y) for a static cable subjected to axial and transverse forces can be written as follows (Mehrabi and Tabatabai 1998):

$$[K]\{y\} = \{F\} \qquad (2\text{-}5)$$

The K matrix is the stiffness matrix with n rows and columns where n is the number of nodes, as shown in Equation 2-6. The elements of the K matrix are shown in Eq.2-6. Parameters Q, S, U, W, V, D, and T are defined in Eq. 2-7 through 2-15. Mehrabi and Tabatabai (1998) provide additional terms for these parameters when there is an intermediate spring (such as a neoprene ring) installed along the length of the stay cable. That term is omitted for the purposes of this analysis.

$$K_{(n\times n)} = \begin{bmatrix} Q & U & W & & & 0 \\ D & S & U & W & & \\ V & D & S & U & - & \\ & V & - & - & - & W \\ & & - & - & S & U \\ 0 & & & V & D & T \end{bmatrix} \qquad (2\text{-}6)$$

$$Q = \frac{1}{2a^4}(-5EI_{i+1} + 22EI_i - 3EI_{i-1}) + \frac{2H}{a^2} \quad \text{, for a cable with fixed end} \qquad (2\text{-}7)$$

$$Q = \frac{1}{2a^4}(-3EI_{i+1} + 18EI_i - 5EI_{i-1}) + \frac{2H}{a^2}$$, for a cable with Pinned end (2-8)

$$S = \frac{1}{a^4}(-2EI_{i+1} + 10EI_i - 2EI_{i-1}) + \frac{2H}{a^2} \quad (2\text{-}9)$$

$$T = \frac{1}{2a^4}(-3EI_{i+1} + 22EI_i - 5EI_{i-1}) + \frac{2H}{a^2}$$, for a cable with fixed end (2-10)

$$T = \frac{1}{2a^4}(-5EI_{i+1} + 18EI_i - 3EI_{i-1}) + \frac{2H}{a^2}$$, for a cable with Pinned end (2-11)

$$D = \frac{1}{a^4}(2EI_{i+1} - 6EI_i) - \frac{H}{a^2} \quad (2\text{-}12)$$

$$U = \frac{1}{a^4}(-6EI_{i+1} + 2EI_i) - \frac{H}{a^2} \quad (2\text{-}13)$$

$$V = -\frac{1}{2a^4}(EI_{i+1} - 2EI_i - EI_{i-1}) \quad (2\text{-}14)$$

$$W = \frac{1}{2a^4}(EI_{i+1} + 2EI_i - EI_{i-1}) \quad (2\text{-}15)$$

Where, K is the stiffness matrix; E is the modulus of elasticity of strand material; I is the moment of inertia of cable cross section; H is the cable tension along the chord; and a is the element length in the discretized cable.

Knowing the K and F matrices, the vector of nodal displacements (y) can then be calculated by solving Eq. 2-5. The nodal displacements can then be used to calculate slopes and curvatures at each node i using finite difference equations.

$$\theta_i = \frac{y_{i+1} - y_i}{a} \quad (2\text{-}16)$$

$$\varphi_i = \frac{M_i}{EI_i} = \frac{y_{i+1} - 2y_i + y_{i-1}}{a^2} \quad (2\text{-}17)$$

The axial strain due to the deformation of the cable under transverse load (ε_a) can be estimated by calculating the cable length under deformed condition (using nodal displacements).

$$\varepsilon_a = \frac{\sum_1^{n+1}\sqrt{a^2 + (y_i - y_{i-1})^2} - L}{L} \quad (2\text{-}18)$$

The single strand cable used in the experiment was discretized with an element length (a) of 1 in (i.e., n = 184). The bending stiffnesses at each element node were calculated using the above equations. The force vector had a single non-zero term corresponding to the mid-length concentrated load. Equation 2-6 was solved using the MATLAB software.

Steps for the finite difference analysis of the 7-wire single strand cable used in the experiment were as follows:

(1) Use the initial tensile force of strand as the tensile force T_i and the vertical force F_t at the target displacement (2.2 in or an effective angle of 25 milli-radians) as the original input value and solve Eq 2-5 to obtain the displacement of the strand at all nodal points.

(2) For the entire strand cable, the stiffness of the strand is taken as I_{max} (full composite action between 7 wires, as shown in Eq. 2-19 and Figure (7). Consider the degree of fixity at the cable ends by adjusting the parameters of formulas (2-7) and (2-8), (2-10), and (2-11).

$$I_{max} = I_{sc} + 6I_{so} + \sum_{i=1}^{7} A_s d_i^2 \qquad (2\text{-}19)$$

Where I_{sc} represents the moment of inertia of the core wire, I_{so} represents the moment of inertia of each outer helical wires, and d_i represents the distance between the centroid of the outer wire and the neutral axis of the strand (Figure 2-8).

The degree of fixity of the cable end should be adjusted to conform with the results of the test. The wedge anchorage system does not provide a fully fixed condition because of the uneven gripping and potential for slippage near the anchorage. By adjusting the parameters, the formula (2-8) becomes:$Q = \frac{1}{2a^4}(-3.15EI_{i+1} + 18.3EI_i - 4.85EI_{i-1}) + \frac{2H}{a^2}$, Formula (2-11) becomes$T = \frac{1}{2a^4}(-4.85EI_{i+1} + 18.3EI_i - 3.15EI_{i-1}) + \frac{2H}{a^2}$. The result obtained is closest to the result of FE, so the apparent degree of fixity is approximately 7.5% for the single strand test.

(3) Solve the axial strain value ε_a according to the displacement curve obtained in step (1), then calculate the axial tension increase (ΔTi) due to ε_a and calculate the final tension force ($Ti+\Delta Ti$). Increase the initial tension and set it as the new tensile force. Repeat the calculations once with the new force.

(4) After obtaining the displacement profile, the curvature (φ) is calculated using the nodal displacements. The total strain due to cable bending (ε_s) is the sum of bending strain (ε_b) and axial strain (ε_a).

$$\varepsilon_b = \varphi d \qquad (2\text{-}20)$$

$$\varepsilon_s = \varepsilon_a + \varepsilon_b \qquad (2\text{-}21)$$

When there is compatibility, bending strain at any point is equal to the curvature times the distance from the neutral axis. The stress developed in strands at any point is equal to the strain due to transverse load times the modulus of elasticity (E = 28,500 ksi).

$$\sigma_s = \varepsilon_s E \qquad (2\text{-}22)$$

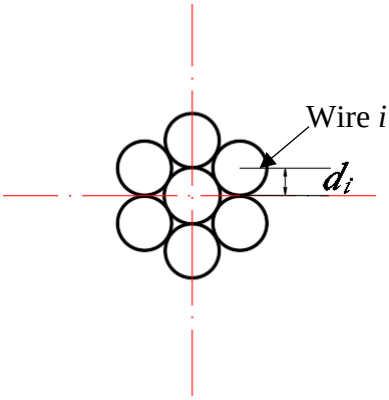

Figure 2-8. Single strand cross section

2.7. Results and Discussion

2.7.1. Experimental results of single strand test

Table 2-3 shows the experimental results from transverse loading of a single strand. The table shows the variation of the strand axial tension (load cell) as a function of vertical displacement at the center point. The table also shows the measured strains on the helical wires 2 in. away from the loading plate (7 in. from the face of the dead-end chuck).

Table 2-3. Results of single strand test under tension and bending

Loading step	Displacement at the middle of the cable, (in.)	Angle change (radians)	Strand Force (kips)	Transverse load (lbs.)	Strain gage 1 (micro-strain)	Strain gage 2 (micro-strain)
0	0	0	18.93	-127	0	0
1	0.22	0.0025	18.96	91	16	12
2	0.44	0.005	19.02	178.9	27	20
3	0.66	0.0075	19.11	271	39	27
4	0.88	0.01	19.24	380	49	37
5	1.10	0.0125	19.39	491	60	45
6	1.32	0.015	19.57	614	76	61
7	1.54	0.0175	19.73	738	89	84
8	1.76	0.02	20.0	866.6	102	120
9	1.98	0.0225	20.22	1000	116	164
10	2.20	0.025	20.55	1136	137	204

As shown in Figures 2-9 and 2-10, the axial tensile force in the strand increased with the imposed displacement at mid-span. The magnitude of the transverse force at mid-span also increased with the imposed displacement. The increased tensile stresses are calculated by taking the load cell increase and dividing by the strand area. Figure 2-11 shows the strain variation with the increase of the imposed displacement.

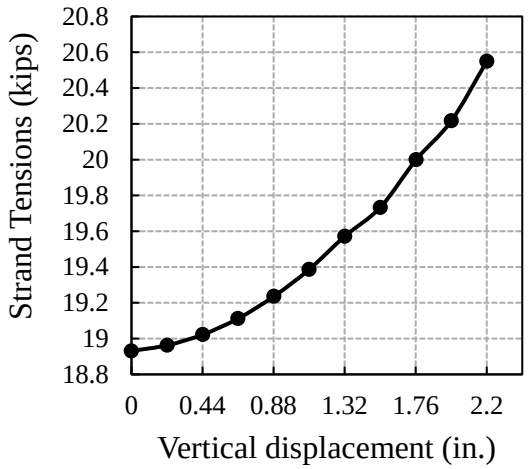

Figure 2-9. Mid-span vertical displacement vs. strand tension in single strand test

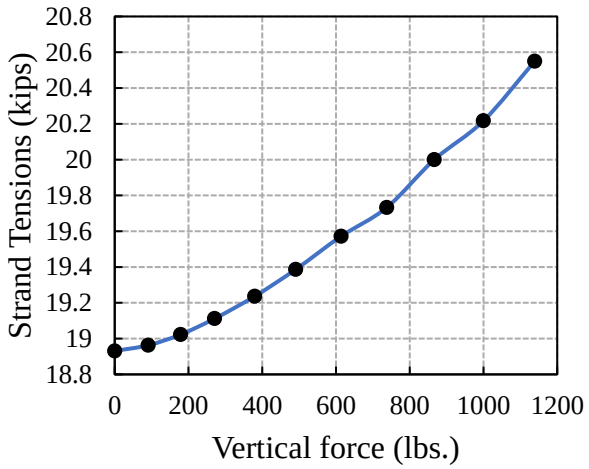

Figure 2-10. Mid-span vertical force vs. strand tension of a single strand stay cable

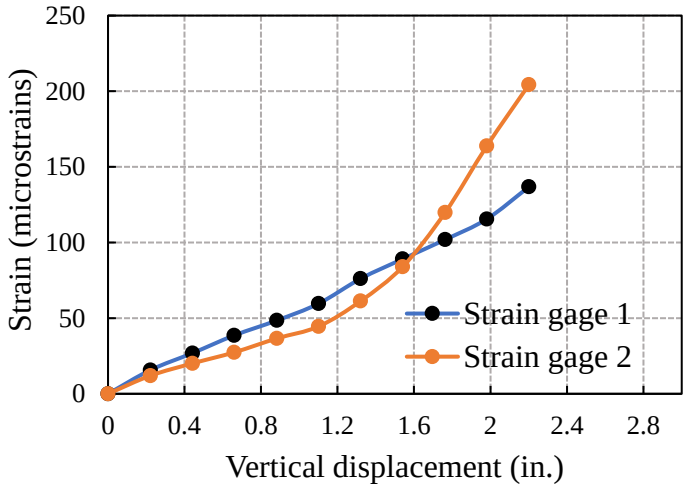

Figure 2-11. Mid-span vertical displacement vs. strains

A simplifying assumption is typically made that the cable can form sharp angles at the anchorages and under the load (Figure 2-12). This assumption is an idealization, and rotation cannot practically occur at the anchorages because they are not hinged connections. The high curvatures at those locations translate into rotations over a relatively short distance, thus

allowing this approximation. Based on this, a relationship can be written between the vertical force P and the cable tension T based on equilibrium of forces at mid-span:

$$\frac{P}{2T} = \frac{\delta}{L_T} \qquad (2\text{-}23)$$

Where δ is the cable displacement at mid-length, α is the inclination angle (in radians), L is the length of the strand, and T is the tension force in the cable. The inclined half-length of the strand can be calculated using the following equation:

$$L_T \sim \sqrt{(\frac{L}{2})^2 + \delta^2} = \sqrt{(\frac{L}{2})^2 + \left(\alpha \frac{L}{2}\right)^2} = \frac{L}{2}\sqrt{1+\alpha^2} \qquad (2\text{-}24)$$

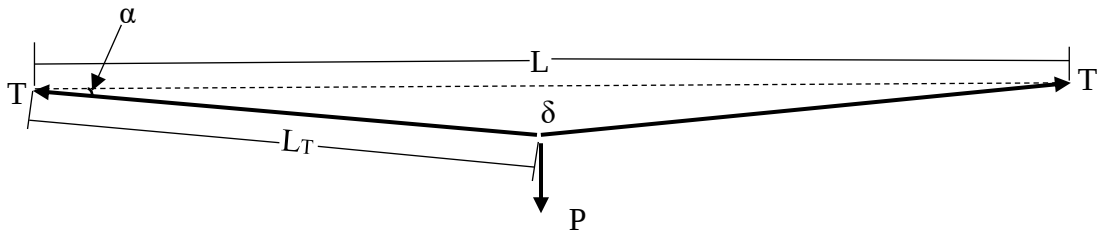

Figure 2-12. Idealized response of a single strand to a transverse force at mid-length

When the inclination angle (α) is 0.025 rad (δ=2.2 in), the measured strand force (T) is 22.5 kips.

$$L_T = \frac{L}{2}\sqrt{1+\alpha^2} = \frac{176.5in}{2}\sqrt{1+(0.025)^2} = 88.28in.$$

$$P = 2T \cdot \frac{\delta}{L_T} = (2)(22500lbs) \cdot \frac{2.2in.}{88.28in} = 1121\ lbs$$

The calculated P of 1121 lbs. is very close to the measured value of 1136 lbs., as shown in Table 2-2.

2.7.2. Comparison of experimental and computational results

Table 2-4 shows axial force results from the experiment and the overall FE model for a strand rotation angle of 0.025 rad. The FE results are in good agreement with the experimental results.

Table 2-4 Comparison of axial forces in the single strand for strand rotation angle of 0.025rad

	Axial force at the beginning (kips)	Axial force after applying vertical force (kips)
Experiment	18.93	20.55
FE (overall model)	19.13	20.12

Figures 2-13 and 2-14 show comparisons of bending stress results from FE and FD method calculations, for strand rotation angles (α) of 0.01 rad and 0.025 rad, respectively. Results from the single strand cable FE model (all seven wires modeled) , the equivalent strand FE model, and the FD model show relatively close agreement. As expected, the maximum bending stress occurs at the support of the cable. There is substantial change in bending stress within a distance of 12 in from the end of the strand. The overall and simplified FE models as well as the results of the FD analyses were in close agreement with each other. However, it should be emphasized that proper boundary conditions (as discussed in sections 2.5 and 2.6) are required in the equivalent model and the FD model to obtain results that are compatible with the full FE model. The bending stresses due to the transverse load obtained by the FE and the FD analyses are very close to those obtained from the experiment.

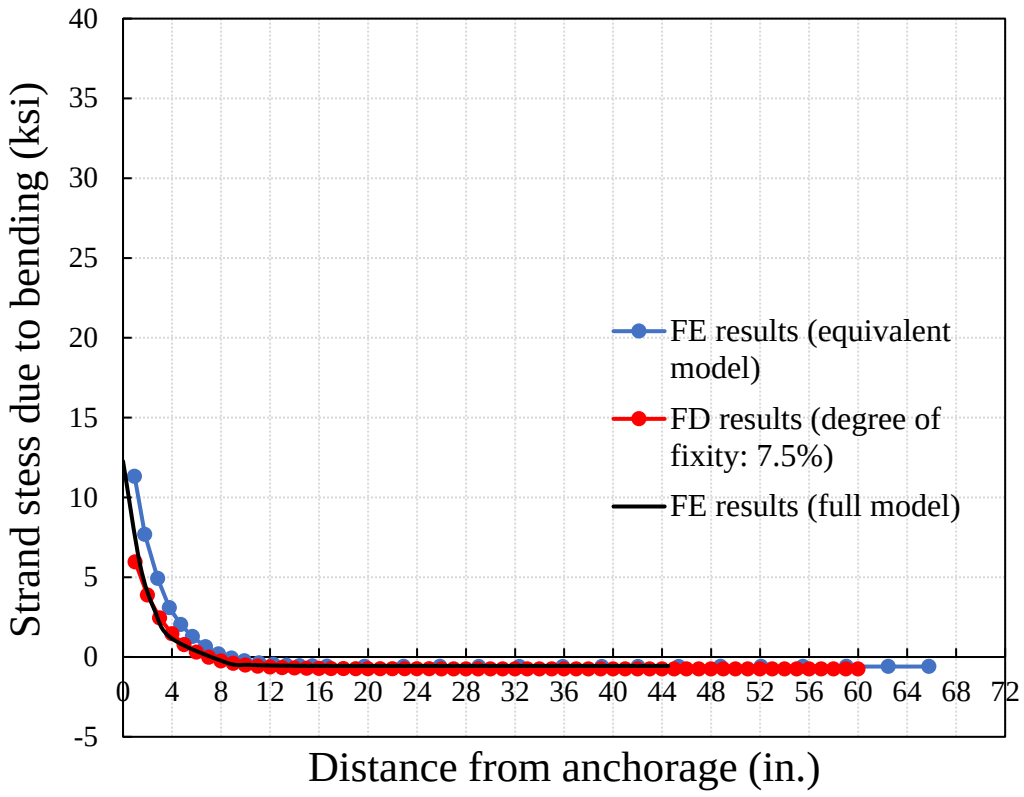

Figure 2-13. Bending stress of single strand stay cable (0.01rad)

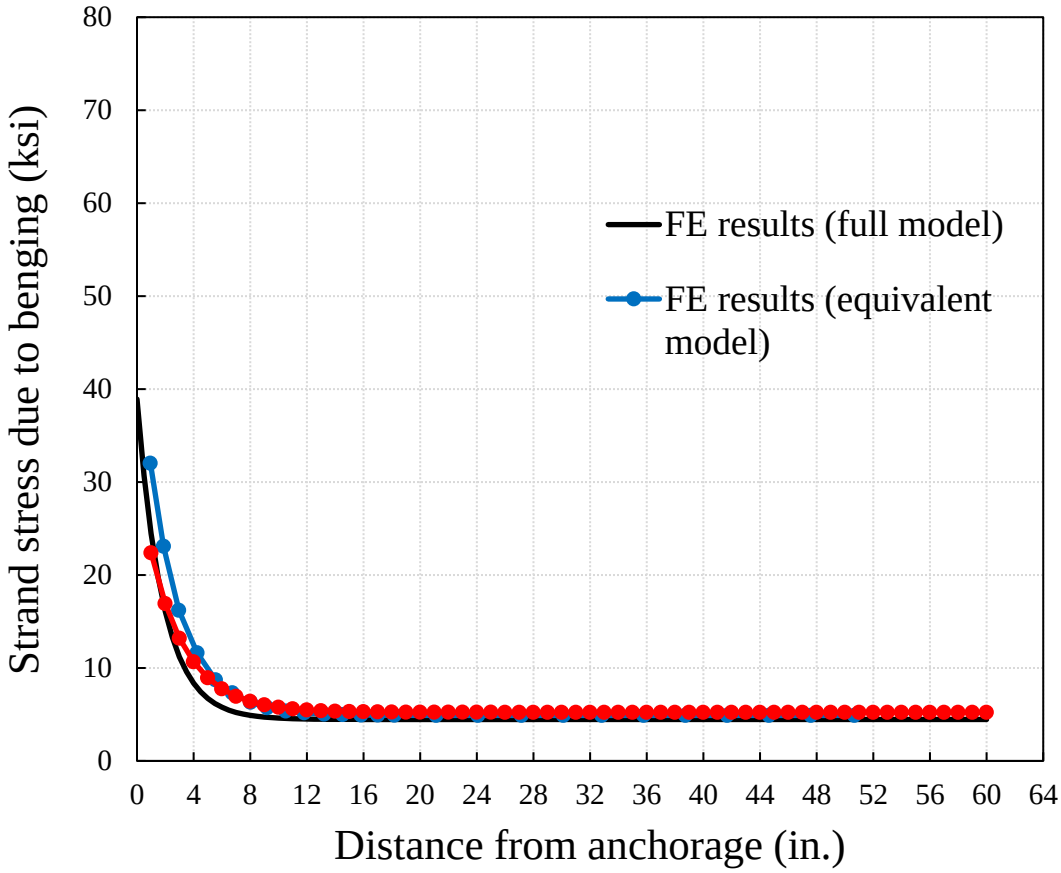

Figure 2-14. Bending stress of single strand stay cable (0.025rad)

By changing the boundary condition parameters in the FD analysis to converge on the full FE results, the degree of fixity of the strand anchorage (2-piece wedge system) can be obtained. The FD boundary condition equivalent to 7.5% fixity was determined to provide the closest agreement to the FE results, while the full model FE results agreed well with the available data from the experiment. The full FE model was also able to properly model the seating of wires in the wedges.

2.8. Conclusions

In this study, a greased-and-sheathed 7-wire strand with a diameter of 0.62 in was subjected to an imposed vertical displacement at its mid-length. The imposed displacement was meant to correspond with apparent rotation angles of 0.01 and 0.025 rad at the anchorage. The bending behavior of the strand corresponding to these displacement levels (rotations) was investigated. To investigate the behavior of the strand after it is tensioned and subjected to a transverse force (bending), a full FE model of the strand including the core and six helical outer wires, the anchorage hardware, wedges, load cell, and the bearing plates used in the experiment were modeled. The results accurately represented the structural response of the strand under tension and bending effects. In addition to the full FE model, an FE analysis of an equivalent cylindrical model of the strand and FD analyses of the strand were carried out to compare with the experimental results.

The equivalent FE model (a solid cylinder) was analyzed to capture the behavior of the strand without the substantial computational cost of modeling all seven wires. An equivalent strand model is needed when trying to model a large number of parallel strands commonly used in stay cables. The equivalent FE model provided results that were reasonably accurate when considering equivalent conditions of the cross-sectional area and moment of inertia. The end surfaces of the equivalent cylinders were partially restrained (with pinned boundary conditions) to properly model the degree of fixity provided by the wedge anchorage system. This meant that the FE nodes within the center region of the cross section (within 40% of the equivalent cylinder) had pinned connections. It should be noted that modeling of wedges and chuck body

in the full FE model allows the seating effects, wire slip, and loss of stiffness to be considered in the full FE analyses.

The application of the FD method provided good agreement with experimental and FE analysis results. The boundary condition modelled in the FD analysis should be equivalent to a 7.5% degree of fixity at the anchorages.

The bending stress is at a maximum at the anchorages, and gradually decreases with distance from the anchorage. The bending-induced stress becomes constant at a distance of approximately 12 in. from the end of the strand. A comparison of experimental and analytical results demonstrated the accuracy of the FE analyses (both full and equivalent models) and the FD method for analyzing cable bending problems. The equivalent FE and the FD models require specific boundary conditions to accurately represent the bending stresses near the wedge anchorages.

The development and verification of the equivalent FE and FD analysis methods can assist with solving the complex problem of bending stresses in strands and lays the foundation for research on the bending of parallel strand stay cables.

2.9 References for Chapter 2

Ceballos, M.A. and Prato, C.A., 2008. Determination of the axial force on stay cables accounting for their bending stiffness and rotational end restraints by free vibration tests. Journal of Sound and Vibration, 317(1-2), pp.127-141. https://doi.org/10.1016/j.jsv.2008.02.048

FIB Bulletins No.89, 2019. FIB BULLETIN NO. 89, Title: Acceptance of stay cable systems using prestressing steels. The International Federation for Structural Concrete (FIB). https://www.fib-

international.org/publications/fib-bulletins/acceptance-of-stay-cable-systems-using-prestressing-steels-pdf-detail.html

Goudreau, S. and Cardou, A., 1993. Flexural testing of an epoxy oversized strand model under traction. Experimental Mechanics, 33(4), pp.300-307. https://link.springer.com/article/10.1007/BF02322145

Huang, X. and Vinogradov, O., 1994. Analysis of dry friction hysteresis in a cable under uniform bending. Structural Engineering and Mechanics, 2(1), pp.63-80. https://www.researchgate.net/profile/Oleg-Vinogradov-2/publication/264020825_Analysis_of_dry_friction_hysteresis_in_a_cable_under_uniform_bending/links/54b3ed990cf28ebe92e43b73/Analysis-of-dry-friction-hysteresis-in-a-cable-under-uniform-bending.pdf

Hong, K.J., Der Kiureghian, A. and Sackman, J.L., 2005. Bending behavior of helically wrapped cables. Journal of engineering mechanics, 131(5), pp.500-511. https://doi.org/10.1061/(ASCE)0733-9399(2005)131:5(500)

Jolicoeur, C. and Cardou, A., 1996. Semicontinuous mathematical model for bending of multilayered wire strands. Journal of Engineering Mechanics, 122(7), pp.643-650. https://doi.org/10.1061/(ASCE)0733-9399(1996)122:7(643)

Khan, S.W., Gencturk, B., Shahzada, K. and Ullah, A., 2018. Bending behavior of axially preloaded multilayered spiral strands. Journal of Engineering Mechanics, 144(12), p.04018112.

Lanteigne, J., 1985. Theoretical estimation of the response of helically armored cables to tension, torsion, and bending. https://ascelibrary.org/doi/full/10.1061/%28ASCE%29EM.1943-7889.0001535

LeClair, R.A. and Costello, G.A., 1988. Axial, bending and torsional loading of a strand with friction. J. Offshore Mech. Arct. Eng. Feb 1988, 110(1): 38-42 (5 pages). https://doi.org/10.1115/1.3257121

Mehrabi, A.B. and Tabatabai, H., 1998. Unified finite difference formulation for free vibration of cables. Journal of Structural Engineering, 124(11), pp.1313-1322.

Nabizadeh, A., Al-Barqawi, M.O. and Tabatabai, H., 2021. Probabilistic Models for Fatigue Resistance of Seven-Wire Prestressing Strands and Stay Cables. Journal of Bridge Engineering, 26(10), p.04021070. https://doi.org/10.1061/(ASCE)0733-9445(1998)124:11(1313)

Papailiou, K.O., 1995. Bending of helically twisted cables under variable bending stiffness due to internal friction, tensile force and cable curvature. Doctor of Technical Sciences thesis, ETH, Athens, Greece. https://www.researchgate.net/profile/Konstantin-Papailiou/publication/265239074_Bending_of_helically_twisted_cables_under_variable_bending_stiffness_due_to_internal_friction_tensile_force_and_cable_curvature/links/573d9eec08ae9f741b2fef60/Bending-of-helically-twisted-cables-under-variable-bending-stiffness-due-to-internal-friction-tensile-force-and-cable-curvature.pdf

Papailiou, K.O., 1997. On the bending stiffness of transmission line conductors. IEEE Transactions on Power Delivery, 12(4), pp.1576-1588. https://ieeexplore.ieee.org/stamp/stamp.jsp?tp=&arnumber=634178

Paradis, J.P.H. and Légeron, F., 2011, October. Modeling of the free bending behavior of a multilayer cable taking into account the tangential compliance of contact interfaces. In Ninth International Symposium on Cable Dynamics (pp. 18-20). https://imechanica.org/files/Paradis&L%C3%A9geron_conf_2011.pdf

PTI DC-45, 2018. Recommendations for Stay Cable Design, Testing, and Installation (DC45.1-18), written by PTI Committee DC-45: Cable Stayed Bridge.

Scanlan, R.H. and Swart, R.L., 1968, January. Bending stiffness and strain in stranded cables. In IEEE Winter Power Meeting.

Raoof, M. and Hobbs, R.E., 1984. The bending of spiral strand and armored cables close to terminations. Journal of Energy Resources. Technology. Sep 1984, 106(3): 349-355. https://doi.org/10.1115/1.3231064

Raoof, M., 1990. Free bending of spiral strands. Journal of engineering mechanics, 116(3), pp.512-530. https://doi.org/10.1061/(ASCE)0733-9399(1990)116:3(512)

Yu, Y., Chen, Z., Liu, H. and Wang, X., 2014. Finite element study of behavior and interface force conditions of seven-wire strand under axial and lateral loading. Construction and Building Materials, 66, pp.10-18. https://doi.org/10.1016/j.conbuildmat.2014.05.009

Chapter 3: Experimental and Numerical Study of Bending Stresses in Parallel Strand Stay Cables

3.1. Abstract

The bundled parallel strand stay cables are important structural components of modern cable-stayed bridges. Strands commonly used in modern stay cables consist of 7-wire greased-and-sheathed strands meeting the requirements of ASTM A416. Stay cables primarily resist tension loads imposed by various loads, but they also resist bending stresses due to wind loads, vibration, and any traverse load applied on the cable. The movements of the deck and towers (at termination points of stay cables) also impose rotations at the cable ends, which will induce bending stresses in the strand bundle. Calculating and analyzing a stay cable's bending stresses is an important consideration, especially with regard to fatigue resistance. Traditionally, designers have assumed a non-composite moment of inertia for the bundle of parallel strands because of the presumed lack of sufficient bond along the length of strands. Therefore, the composite effect is generally not considered, and the moment of inertia is typically assumed to be equal to the number of strands times the moment of inertia of an individual strand. This assumption neglects the fact that relative slippage between strands cannot occur because the anchorage plates enforce compatibility at cable ends. Also, periodic cable bands (tying of the strand bundle together) along the free length of the cable may provide some degree of composite action. This study examines the bending stresses developed near the termination points of stay cables due to the application of transverse loads on the cable. Experiments and computational analyses are conducted to assess these bending stresses. The computational models are verified using laboratory experiments performed on a 5-strand cable. Detailed and

simplified finite element models were developed. Theoretical solutions based on a finite difference method are also evaluated and used to develop proposed equations for calculating bending stresses. Bending stress calculation procedures are developed using a simplified stay cable model.

Keywords: Stay cables; Bending stress; 7-Wire strands; Finite element method; anchorage

3.2. Introduction and literature review

The Post-Tensioning Institute (PTI) standard on stay cables (DC-45 2018) and the International Federation for Structural Concrete Bulletin No. 89 (fib 2019), as well as others, have traditionally implied that the bending stresses at the anchorage of a stay cable can be represented by an apparent angle change introduced due to loading (i.e., assuming zero bending stiffness in the cable). The governing US standard for the design of stay cables (PTI DC-45 2018) specifies that an angle change of 25 milli radians "occurring at the entrance of the stay cable into the anchorage or at any other location in the anchorage where the stay cable may be assumed to be deviated" should be the basis for assessing the bending strength of stay cable at the anchorage.

Designers have traditionally ignored the potential composite action in stay cables between 7-wire strands in a parallel strand bundle except when grouted strands are used. The PTI standard (DC-45 2018) states: "For individually protected MTE [main tension element] without grouting of the stay cable, the stiffness may be assumed as the sum of the stiffness of each individual MTE." This means that no composite action should be assumed, and the cable should be considered a set of independent strands when considering bending stresses in cables.

The same approach is taken for bending qualification tests of stay cable anchorages. The fib Bulletin No. 89 (fib 2019) specifies cable bending test requirements that are based on the imposition of angle changes of ±10 milli radians for 100,000 cycles followed by ±25 milli radian angle changes for 2 million cycles. This approach considers that angle change is a measure of bending stress regardless of the size of the cable or its length.

The Texas Department of Transportation (TxDOT) special specification (Special Specification 4064 stay cables, 2004) stipulates that the angle change in the anchorage or transition zones should not exceed 0.025 radians. It also specifies that the bending stress in each strand should not be larger than 36 ksi in the transition zone at the entrance to the anchorage.

Considering that each strand in a multi-strand stay cable terminates at a rigid anchor head/bearing plate, and the cable end connection is not hinged, the angle change cannot occur right at the anchorage. Instead, angle change occurs over a distance (typically within the transition zone). Transition zone is the area near the anchorages where strands are slayed out (separated) from the bundle, with each strand individually anchored at the anchor head. Within the transition zone, the strands are fully separated from each other, but they are still constrained at the anchorage. Relative slippage between strands cannot occur at the anchor head, but the strands can bend individually within the transition zone. While using angle change as a measure of bending stress is simple and convenient for designers, its accuracy, or lack thereof, has not been established for cables of various sizes and length. The consideration of angle change as a single measure of bending stress would imply that short, long, small, and

large cables would all result in the same bending stress if the imposed angle change were the same.

The calculation of bending stiffness for a non-composite parallel strand cable is based on the superposition of the stiffnesses of each strand with respect to their local neutral axis. The PTI DC-45 standard considers that the bending stiffness of parallel strand cables is equal to the stiffness of individual strands times the number of strands (PTI 2018). In modern stay cables, the cable is a bundle of greased and individually sheathed 7-wire strands that are splayed out near the anchorages and terminate in anchorage plates (Nabizadeh et al. 2021). The premise of the PTI DC-45 approach is that the bond between individual strands is non-existent, and therefore an assumption of no composite action can be valid. If it is assumed that there is no bond between the strands, then each strand would act (and bend) separately, and then I could be calculated using the equation (1-5).

$$I = n \times I_s$$

The upper bound of EI corresponds to the condition where all strands work as a whole (fully composite). The composite moment of inertia can be calculated using the following equation.

$$I_c = n\, I_s + \sum A_s \cdot d^2$$

Fürst et al. (2001) studied bending stresses in stay cables under different axial force and rotations of the cable ends. The authors reported that the bending stress can be reduced by properly rotating the position of the anchor relative to the chord, guiding the cable at the end of the anchor, and providing sufficient rigid support at a length (guide length) from the anchor. The authors also provide suggestions for proper guide lengths and stiffnesses. When calculating

the moment of inertia of the cable, it was assumed that the stay cable was composed of n parallel strands that can freely slide. Composite action between strands was not considered.

Prato et al. (2003) studied the dynamic bending stress of stay cables under two conditions: (1) cement grout injected into the cable duct along the length of the stay cable; (2) the socket attachment was not filled with grout, and there was no guides or transverse support. Near the anchorage, bituminous epoxy was used instead of grout. The maximum dynamic stress in continuously grouted cables were lower than those of ungrouted cables, where the maximum dynamic stress was generated by both global and local bending. To calculate the moment of inertia of the strand bundle at this zone, the authors used the moment of inertia of an equivalent circular section multiplied by a cross-sectional porosity, with the bending and shear stiffnesses of the cable being considered as a composite effect.

Caballero (2010) study stay cables that are made up of a bundle of parallel seven-wire strands with a transition zone, pointed out that if a cable was anchored at a fixed end, the forces at the anchorage can be obtained using the following equation:

$$M_{FE} = \sqrt{EIT}\sqrt{\sin(\alpha)\tan(\alpha)} \qquad (3\text{-}1)$$

Where H is the horizontal reaction force, T is the axial force, M_{FE} is the fixed-end reaction moment, α is the inclination of the stay cable, E is the Young's modulus of the stay cable, I is the moment of inertia of cable. The bending stress in a wire can be calculated using the following equation: $\sigma_B^{max} = 2\alpha\sqrt{\lambda E f_{UTS}}\sqrt{\sin(\alpha)\tan(\alpha)}$, where , λ is a loading parameter, and f_{UTS} is the ultimate tensile strength of the cable material. When the curvature caused by the loading is small, the wire slippage can be ignored, and the bending stiffness can be calculated based on an assumption of fully composite behavior. When the loading is large and produces a

large α, all wires need to be regarded as an individual component due to their slippage, the stiffness, and the overall stiffness is considered as the sum of individual wire stiffness.

Winkler et al. (2015) conducted an experimental study of the cyclic bending of multi-strand stay cables to establish a relationship between the reverse cyclic bending behavior of single-strands and that of a multi-strand stay cable. The test applied axial loading and lateral displacement. The deformations of the strand surface and the wires were measured using the digital image correlation (DIC) technique. The relationship between transverse stiffness and the change in tensile force for single and multiple strands was investigated. In the multi-strand cable specimen, the contact pressures and bending effects received by the monostrand located at the center of the cable were different from those of the outermost monostrands. The outer strands were more stressed.

Large amplitude vibrations of stay cables are not uncommon. Shen et al. (2022) established an analytical model for the bending fatigue life of low-sag cables under harmonic loads, which was used to predict the fatigue life of cables in the anchorage zone. The results show that using a guide deviator can significantly prolong the fatigue life of cables in the anchorage. The bending stress at the extreme fiber of the cable at the location of guide deviator was calculated using the following formula:

$$\sigma_b = \beta_G \phi r \sqrt{ET_s/I} = \beta_G \phi E \left(\frac{r}{r_g}\right) \sqrt{\varepsilon_s} \qquad (3\text{-}2)$$

where r is the distance between the extreme fiber and the neutral axis, and r_g is the radius of the gyration of the section. T_s is the static tension, I is the moment of area, ε_s is the static strain, β_G is a coefficient such that $M_G = \beta_G M_{max}$, M_G is the bending moment at the guide

deviator, and ϕ is the total angular deviation. $M_{max} = \emptyset\sqrt{EIT_s}$ It was considered that slip has little influence on the bending stress of extreme fiber, so the non-slip assumption was adopted.

In general, the existing studies have differing approaches for considering the bending stiffness of parallel strand stay cables. When it is believed that there is no slip between strands, it is possible to use the composite bending stiffness. If there is no friction or contact between the strands (e.g., within the transition zone), then the conservative approach of simply summing up the stiffness of each strand is theoretically acceptable. However, this approach ignores the fact that the anchorage plate in parallel strand stay cables can enforce displacement compatibility ("plane section remain plane") at the anchor head. This would result in different forces developing in the strands (based on distance from the center of the strand group) even though the strands are separate from each other. When considering the bending stiffness of multi-strand (parallel strand) stay cables, the extent of composite action in the strand bundle and the mechanisms for bending moment resistance (especially in the transition zone) need to be determined. This study aims to address these questions and develops a calculation process based on experimental and computational research.

3.3. Five-strand stay cable experiment

A test setup was designed and built to test the validity of the common assumption of independent (non-composite) action of strands in parallel strand stay cables. A 5-strand cable was tensioned in a reaction frame (consisting of two steel reaction beams and a set of bearing plates), and then subjected to a transverse load at its mid-length. Five 7-wire greased-and-sheathed strands (0.62 in. diameter) from an actual cable stayed bridge project were used in

the test. An angular deviation of up to 0.025 radian was imposed on the cable at the anchorages through the vertical load. The test setup is shown in Figure 3-1. If all five strands developed the same load increment due to the application of transverse load, the assumption of non-composite (independent) action would be verified. If, on the other hand, the force increments in the strands form a linear distribution with respect to their vertical position in the cross section, then some level of composite action exists between the strands and the assumption of fully non-composite action commonly made in design would be invalid.

All strands had individual center-hole load cells at the dead-end side of the cable. Two-piece wedges (designed for stay cable anchorages) were used in chucks at the live and dead ends of the cable. Two cylindrical steel tension rings were used at the ends of the transition zone near both anchorages with a transition length of 26 in. Another steel cylinder (same dimension as the tension ring) was used under the applied transverse load. Ten resistance strain gages were attached to the outer wires of strands (two at each strand) near the anchorage. A sketch of the test setup and location of strain gauges are shown in Figure 3-2. The strands were individually stressed and seated using a center-hole hydraulic jack, jacking chair, and steel shims as needed to reach a load of approximately 30% of the minimum ultimate tensile strength (MUTS) of 270 ksi. The load cells under the dead-end chucks of all strands (Figure 3.3c) allowed continuous monitoring of strand force changes during transverse loading.

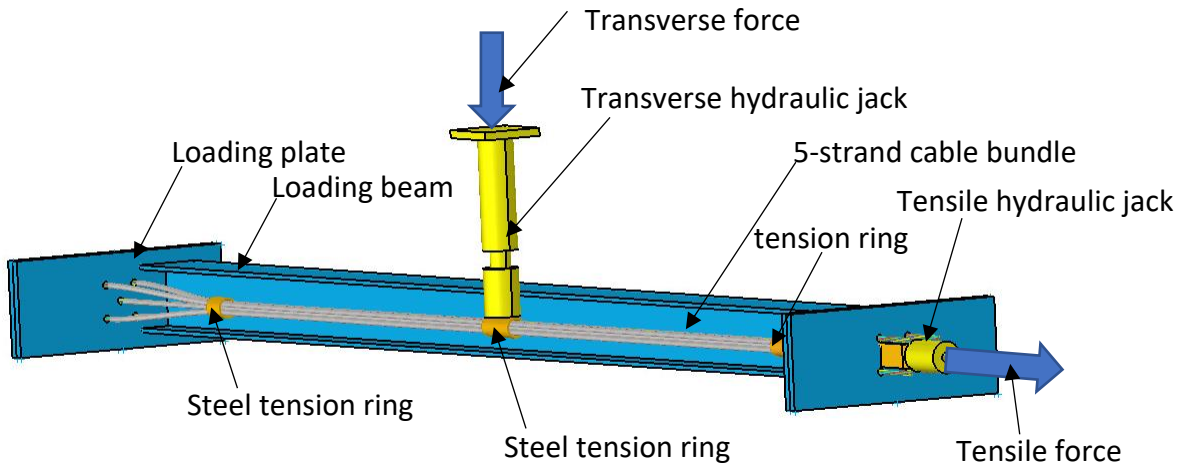

(a) Loading setup for 5-strand cable

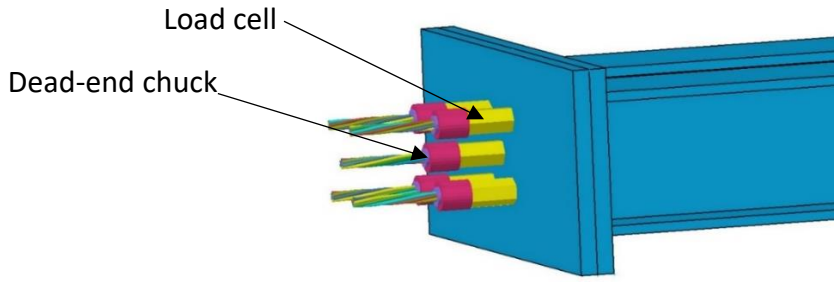

(b) Dead end of 5-strand cable

Figure 3-1. Loading setup for experiments

To assemble the 5-strand cable, the polyethylene sheathing on the individual strands was removed in the end regions, as seen in Figure 3-3. A vertical hydraulic jack was used to impose a transverse displacement at the mid-length of the cable, with the displacement measured using an LVDT and the force measured using a load cell. A steel ring (cylinder) similar to the deviation rings used at the ends of the transition zones was used around the cable bundle at mid-length. A steel plate was welded on top of the ring to facilitate the application of transverse load to the

cable (Figure 3-4e). The imposed displacements were applied in increments. Of particular interest were displacements corresponding to apparent angular rotations of 0.01 and 0.025 radians. These rotations were identical to those applied in the single-strand test described in Chapter 2.

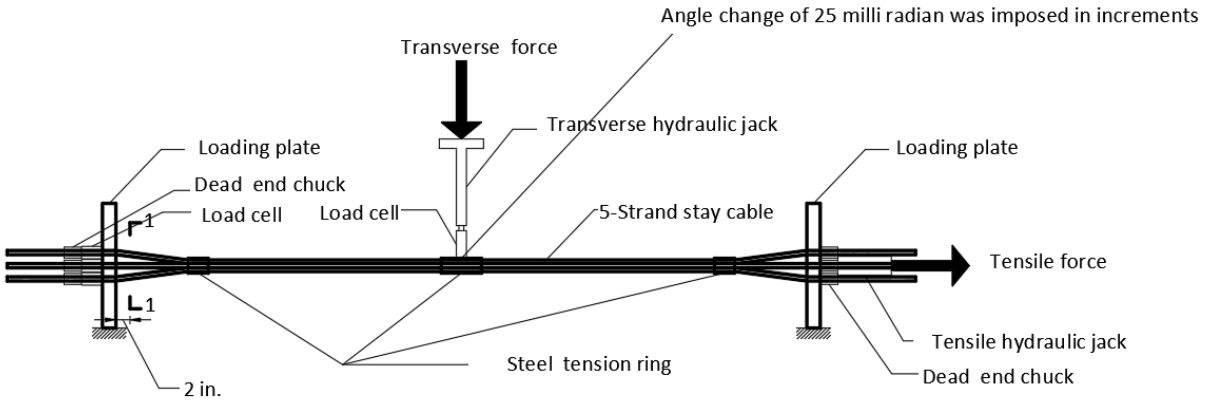

(a) Test setup sketch

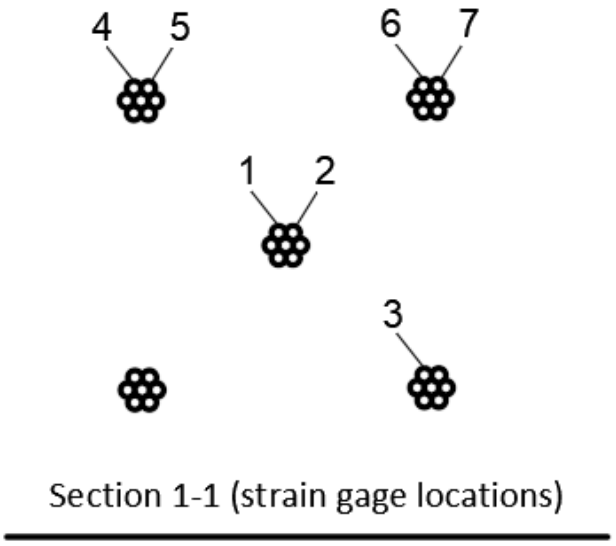

(b) Strain gage location

Figure 3-2. Test setup sketch and strain gage location for 5-strand specimen

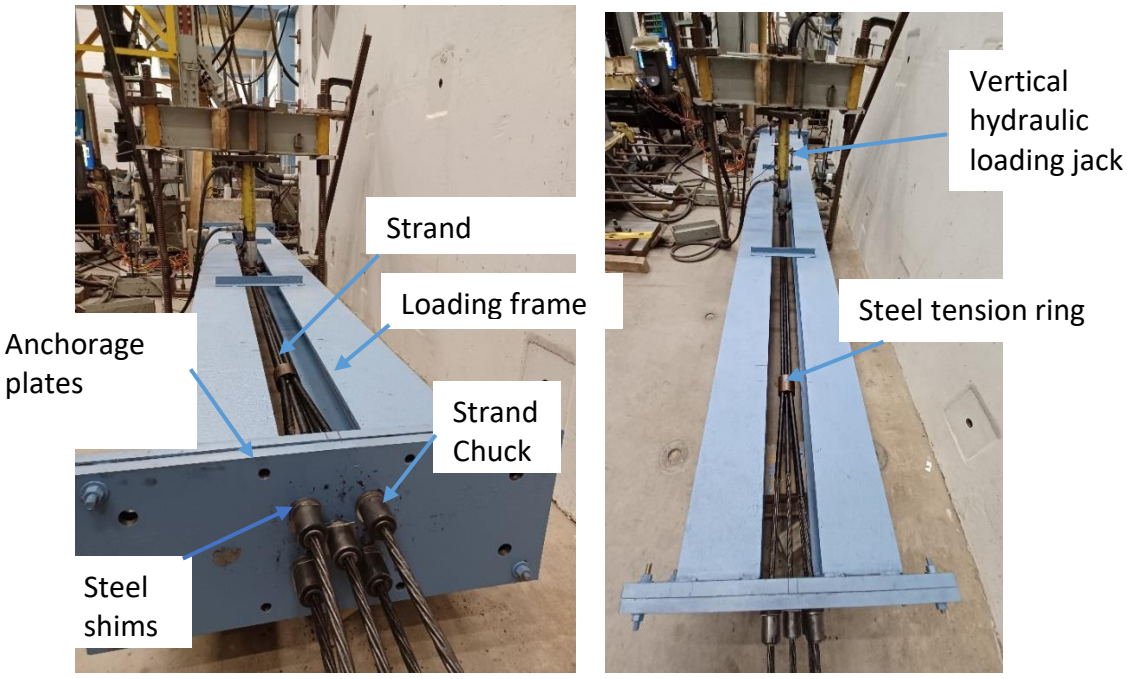

(a) Test setup （live end chucks with steel shims） (b) Test setup for 5-strand cable test(top view)_ (2)

(c) Test setup for 5 strands (side view)

Figure 3-3. Actual test setup for 5-strand specimen

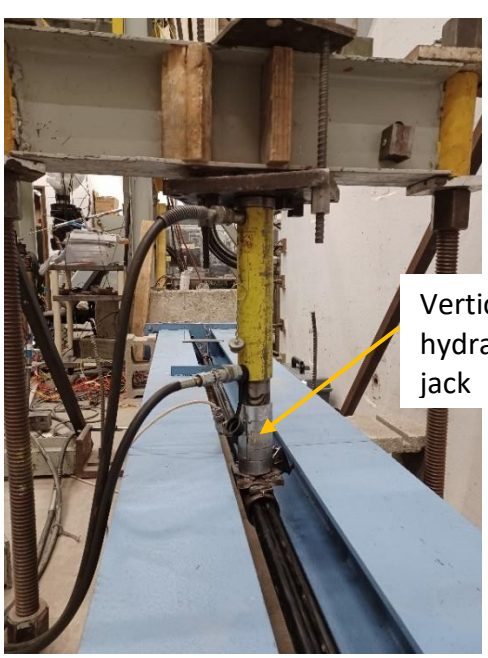

(a) Vertical hydraulic jack

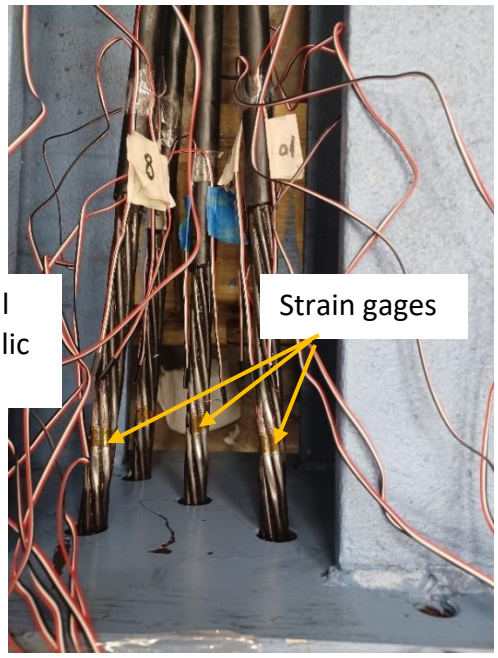

(b)Strain gage locations strands

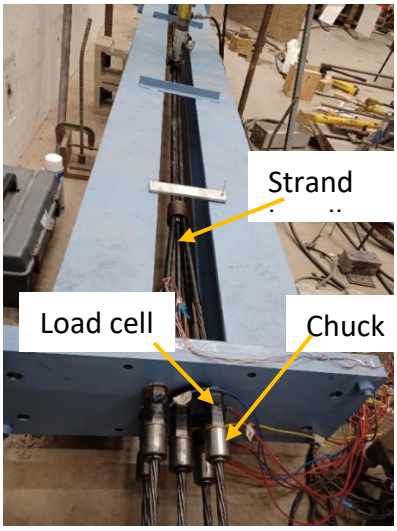

(c) Dead end of the cable

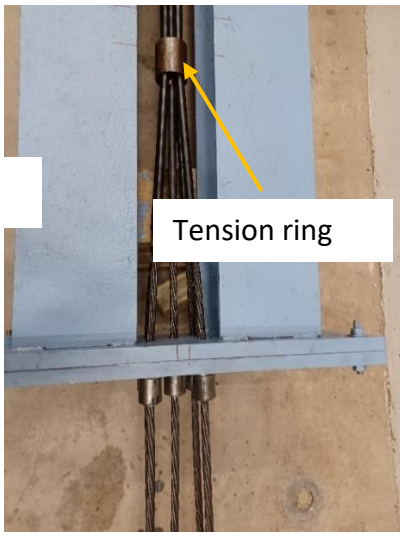

(d) Live end of the cable

(e) Connection of vertical jack with cable

Figure 3-4. Details for test setup

3.4. Finite Element Analysis

The Altair finite element program was used to model the 5-strand cable test. The feasibility and effectiveness of using an equivalent cylindrical model for strand was established in finite element models of the single strand cable presented in Chapter 2. To simulate the behavior of the 5-strand cable used in the experiment, each strand was modeled as an equivalent cylinder (Figure 3-5). The polyethylene coating was also modeled. The polyethylene coating was not used in the end regions since the coating was removed in that area during the test. The model consists of five equivalent steel cylinder models and high-density polyethylene covers. One-half of the cable was modeled with boundary conditions representing symmetry used at the center of the cable As in the experiment, a steel tension ring was modeled at a distance of 26 in. from the end of the strand (cable end of the chuck in the experiment) as well as in the middle of the span. The tension rings allowed the strands to splay out from a bundle in the free length to the hole pattern at the anchor head.

The friction coefficients between the steel strand and the polyethylene sheathing, and between two polyethylene sheathed strands (strand contact) were assumed to be 0.2 (Engineering ToolBox, 2004). The penalty-based contacts were defined as well.

The analysis method used in the Altair software was nonlinear static analysis. The stress-strain behavior of the 7-wire low-relaxation prestressing strand used in the model is shown in Figure 3-6 (obtained from the PCI design handbook). The yield strength was 270 ksi with an elastic modulus of 28,500ksi. Eight-point 3-dimensional pyramid solid elements were employed. The element size was 0.118in. (0.003m).

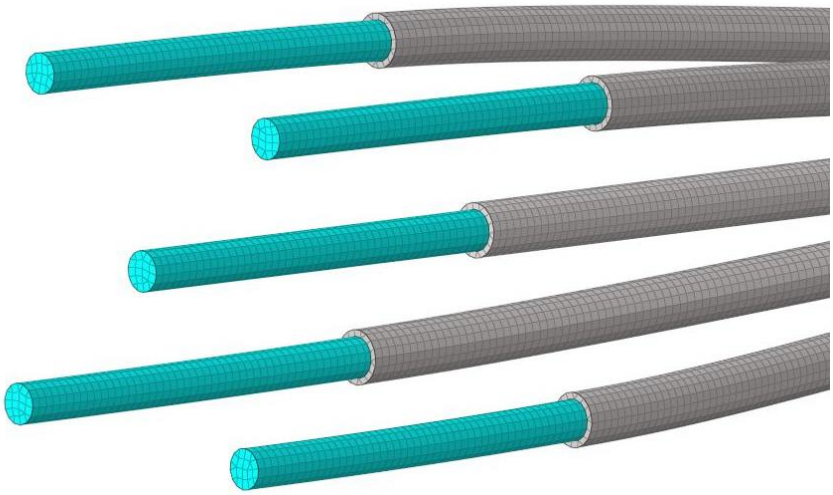

Figure 3-5. FE Mesh for the 5-strand stay cable model

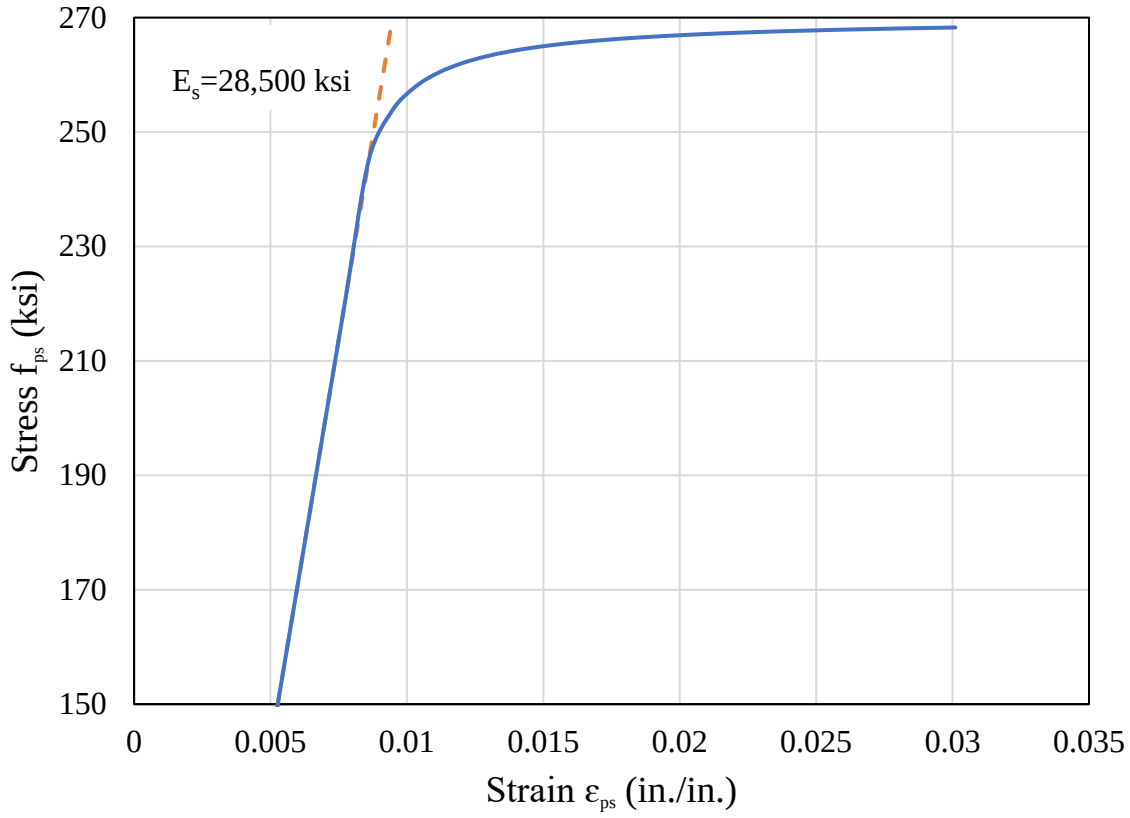

Figure 3-6. Stress-strain curve of the 7-wire low-relaxation prestressing strand (Adapted from PCI design handbook)

The boundary conditions for the equivalent strand model included pinned support at three center nodes at the end face of each equivalent cylinder (Figure 3-7). This partial restraint of the end of the strand model was developed in Chapter 2 to properly represent the end moments in the strand. The restrained nodes cover the central 40% of the diameter of the equivalent cylinder model. The overall model can be seen in Figure 3-8.

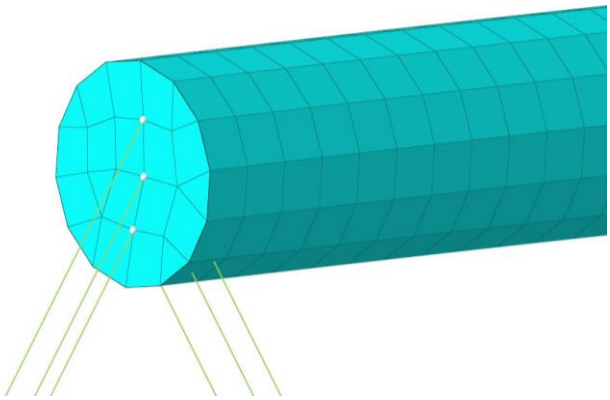

Figure 3-7. Pinned support boundary condition

(a) Symmetrical model of a 5-strand model

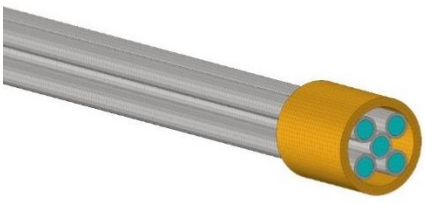

(b) Symmetrical center of the half model for the strand

Figure 3-8. FE model of the 5-strand model

The initial axial stress in the cable corresponds to the initial tensile stress in the test strands, which was simulated in the FE model by applying a virtual cooling temperature change to the strands. Then, a vertical displacement of 2.2 in was applied at mid-span of the cable, (corresponding to a rotation angle of 0.025 rad).

3.5. Results and discussion

3.5.1 Results of 5-strand stay cable test

Table 3-1 shows the results obtained from the 5-strand cable test as the imposed transverse displacement was incrementally increased from zero to an angle change of 25 milli radians (2.2 in). The strand numbers are shown in Figure 3-9.

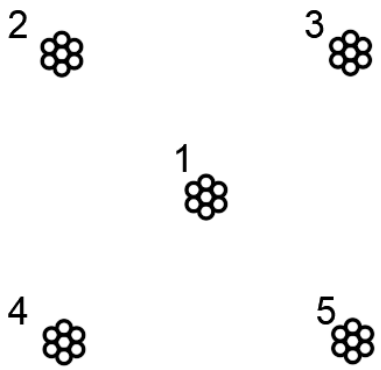

Figure 3-9. Strand bundle cross section and numbers of the strands looking towards the dead end

Table 3-1. Test results of 5-strand bundle specimen under tension and bending

loading step	Displacement at the middle of the cable (in.)	Strand force (load cell) (kips)					Transverse load (lbs.)
		1	2	3	4	5	
1	0	17.43	19.07	18.41	17.23	16.62	4
2	0.11	17.44	19.17	18.51	17.16	16.49	194.8
3	0.22	17.46	19.26	18.58	17.12	16.41	360.4
4	0.44	17.51	19.46	18.74	17.04	16.28	735.3
5	0.66	17.58	19.70	18.94	16.94	16.13	1168.0
6	0.88(0.01rad)	17.70	19.92	19.12	16.86	16.0	1600.1
7	1.10	17.86	20.18	19.34	16.76	15.88	2121.1
8	1.32	18.04	20.51	19.62	16.65	15.77	2734.0
9	1.54	18.25	20.81	19.92	16.57	15.66	3300.6
10	1.76	18.49	21.16	20.23	16.50	15.58	3893.9
11	1.98	18.76	21.54	20.60	16.45	15.53	4529.1
12	2.20 (0.025rad)	19.04	21.90	20.98	16.43	15.51	5184.2

Figures 3-10 through 3-11 show that the stresses in the top strands increased with increasing transverse displacement, and stresses at the bottom strands decreased with the increasing transverse displacement (bending moment). The increased/decreased tensile stresses are calculated by dividing the individual load cell increments by the strand area. This observation clearly indicates that the strands in the cable within the transition zone are not independent since a non-composite (independent) action would have resulted in the same stress increments in all strands. The individual strands, in fact, act together to resist the imposed bending moment. This illustrates the partially composite behavior of strands within the transition zones near the anchorage. Although there is no bond (contact) between strands within the transition zone, the strands are not acting independent of each other. The strands

force variations are not the same and are a function of the position of strands. The transverse load increases the axial stress in the entire cable as well. That is reflected in the increase in the center wire with increased transverse displacement. Therefore, assumption of fully non-composite action (i.e., independent strands) is not valid.

Similarly, the axial tension in the top two strands increases with an increase in the vertical displacement at mid-length of the cable. The axial force in the central strand also increases (less than the increase in top strands), but the axial tension in the bottom two strands decreases. This also reflects some composite action between the strands. The sum of the initial tensile force in all five strands was 88.75 kips. However, when the mid-span displacement reached the maximum level imposed (2.2 in.), the total force increased to 93.86 kips.

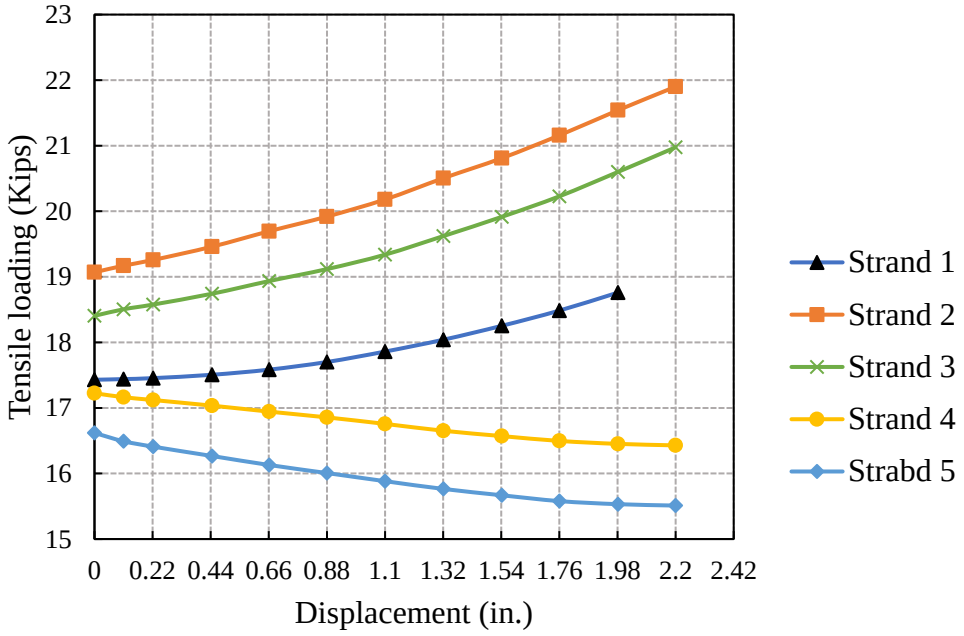

Figure 3-10. Variation of measured strand force vs. applied displacement

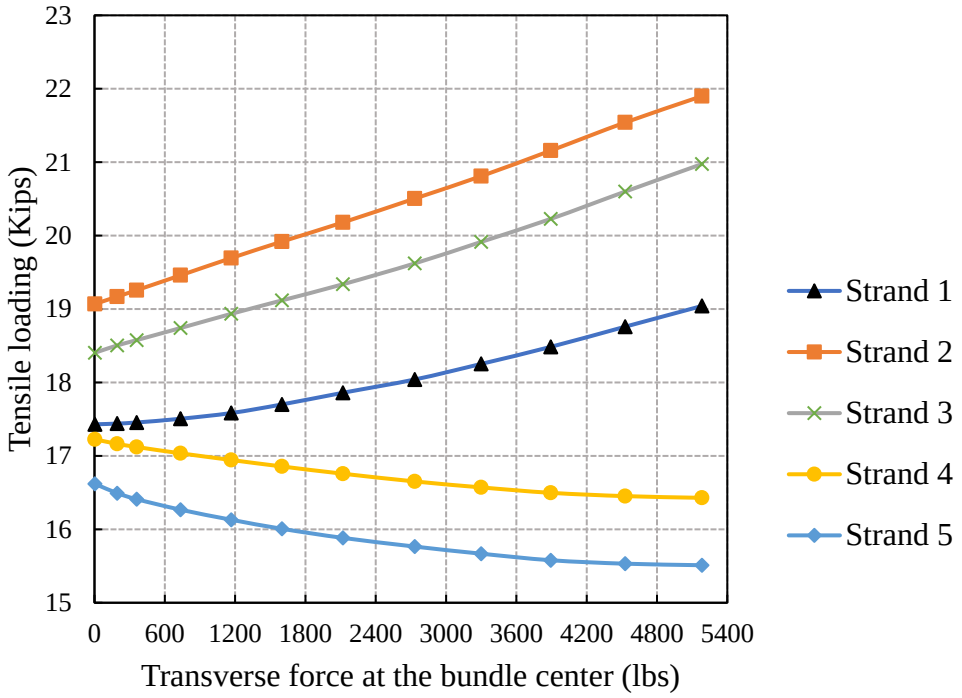

Figure 3-11. Strand force variation with transverse force.

3.5.2. Comparisons of experimental results with FE model

A summary of the results can be seen in Table 3-2. The experiment and FE results show that, with the application of transverse load, the total axial force in the cable bundle increases, but the increase is not the same in all strands. The axial forces increased the most in the top two strands. There was also an increase in force in the center strand. However, forces in the bottom strands decreased with increasing transverse displacement. Table 3-2 shows that strand forces predicted using the FE model were close to the experimental results. The original (before application of transverse load) total tensile force in the cable bundle was 88.74 kips (from test) and 89.20 kips (from FE result), with a difference of 0.5%. After applying the transverse

displacement corresponding to a rotation angle of 0.025 rad, the cable tension increased to 95.86 kips (from test) and 98.2 kips (from FE result), with a difference of 2.4%.

As strands are tensioned, the wedges move and grab the strands. There are, therefore, seating losses associated with the initial tension of the strands. The center strand has been previously used in the single strand test (described in Chapter 2) and had previously experienced higher tensile force (than the initial force). Therefore, additional seating losses would not be expected for the center strand during the loading. The two lower strands exhibited a force reduction and would therefore not be subjected to additional seating losses. The top two strands are expected to exhibit additional seating losses since these strands were not pre-seated before the test. Since the FE model of five equivalent strands did not consider the slip effect of the strand at the wedges, the slip displacement data obtained from the full FE model of the helical single strand (Chapter 2) to calculate a correction for axial force of the top strands considering the effect of strand seating loss. The single-strand model included modeling of friction between the wedges and individual strand wires, thus allowing the seating loss estimates to be made.

Table 3-2 compares the strand force as determined experimentally and estimated using the FE model. The experimental results are in close agreement with the FE results for the center (core) and bottom strands. However, the top strands show a diversion. When subtracting the estimated slip strain (seating loss divided by half the cable length) for the two top strands, the axial force (corresponding to 0.025 rad angle change) would become 95.42 kips, with only a 0.46% difference between the experimental result and adjusted FE results.

The transverse load required to achieve the 0.025-radian rotation in the FE model was 5.34 kips, while the corresponding experimental force was 5.15 kips. The difference of 3.7% indicates good agreement between the experimental and FE results.

Table 3-2. Summary of experimental results – 5-strand cable test (considered the seating loss effect)

Strand location	Original tensile force (kips)		Tensile force after bending (kips)		Transverse force (kips)		Rotation angle (Rad)
	Test	FE	Test	FE	Test	FE	
Entire cable	88.74	89.2	95.86	98.2* /95.42	5.15	5.34	0.025
Top	18.74	18.68	21.43	21.354	—	—	
Core	17.43	17.42	19.04	19.36	—	—	
Bottom	16.92	17.19	15.97	16.70	—	—	

*Without considering seating losses.

Figure 3-12 shows the change in the experimental bending stresses due to the application of transverse load in the top, core, and bottom strands corresponding to an imposed angle change of 0.025 radians. This indicates that the strand bundle (even in the separated condition within the transition zone) does not act as an independent set of strands, as assumed in PTI DC-45 and fib Bulletin 89 standards. The increase in the center strand stress in the 5-strand test (6.95 ksi) is very close to the corresponding stress change in the single-strand test (6.98 ksi) (Chapter 2). A comparison of maximum strains (FE and experiment) is shown in Figure 3-13. The same linear behavior is observed on both, i.e., no independent strand response.

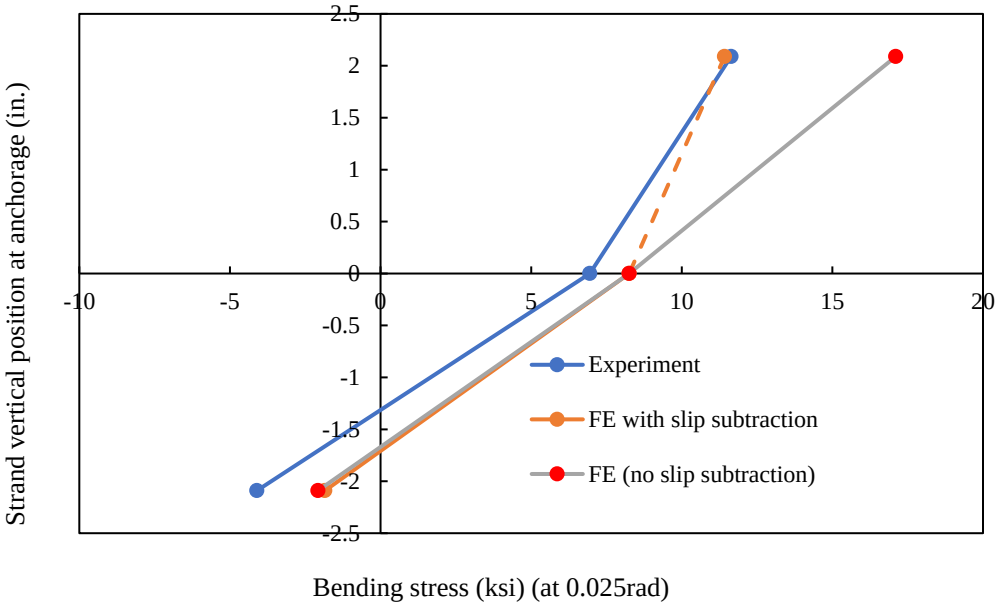

Figure 3-12 Comparison of FE and experimental bending stresses at different strand positions (0.025 radian rotation)

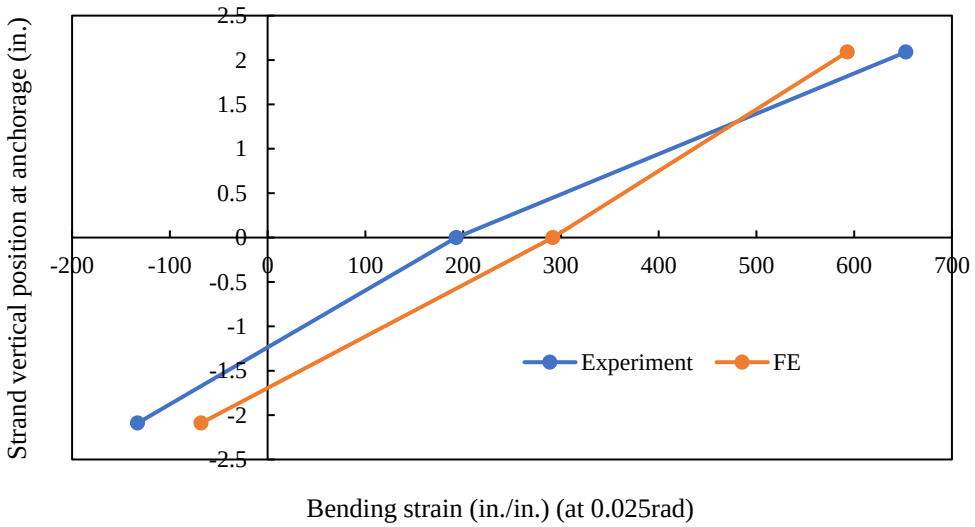

Figure 3-13. The bending strain comparison (0.025rad)

To determine whether the level of friction between strands affects the stress level in strands, the 5-strand FE model was repeated for friction coefficients (μ) of 0.05, 0.20 and 0.50. Table 3-3 shows the strand stresses (top, core, and bottom) for FE models with various friction

coefficients between the strand and sheathed cover (polyethylene) and between the sheathed cover and tension rings in the 5-strand model, corresponding to a rotation angle of 0.025 rad. It can be seen that the differences in strand stress are small. Therefore, friction coefficient has a limited effect on the bending stress in strands.

Table 3-3. Average bending stresses in the top, core, and bottom strands with different frictional coefficients setting at 0.025rad.

Frictional coefficient (μ)	Top strand (ksi)	Core strand (ksi)	Bottom strand (ksi)
0.05	17.83	17.84	17.73
0.2	8.62	8.72	8.53
0.5	-2.12	-3.12	-1.66

The In-plane bending moments developed at the anchor head (M_1) and at the tension ring (M_2), can be estimated as the sum of the force in each strand times the vertical distance from the center of that strand to the centroid of the cable cross section at each location.

$$M_1 = T_{s1}d_{11} + T_{s2}d_{21} + \cdots - T_{s(n-1)}d_{(n-1)1} - T_{sn}d_{n1} + M_{s1} + M_{s2} + \cdots + M_{sn}$$

$$M_1 = \sum_{i=1}^{n} T_{si}d_{i1} + \sum_{i=1}^{n} M_{si}d_{i1}$$

Similarly,

$$M_2 = \sum_{i=1}^{n} T_{si}d_{i2}$$

Where T_{si} is the tension force in the i^{th} strand.

n is the number of strands in the cable

d_{i1} and d_{i2} are distances between the i^{th} strand and the center of the cable at the anchor head and the tension ring, respectively.

It can be concluded that the bending action generated by the transverse force applied on the cable will increase the axial force of the 5 -strand cable bundle. However, the change in force is different in each strand based on their vertical position at the anchor head. The axial force in the top strands increases, while the axial force in the bottom strands decreases. Thus, this apparent composite effect must therefore be considered in design, and changes must be made in relevant design specifications. In addition, the FE model of the multi-strand cables using equivalent cylinder models of strand can accurately reflect the bending behavior of the cable.

3.6. Conclusions

Experimental and computational research was performed on a 5-strand stay cable specimen. In the experiment, each strand was stressed to about 30% of the minimum ultimate tensile strength of 270 ksi. Subsequently, a vertical force was applied at the mid-length of the cable to impose bending stresses and deformations. The resulting stresses and strains in each strand were measured using load cells and strain gages. Finally, FE computational models were developed, which were verified using the experimental results.

Results show that the top, center, and bottom strands have different stresses under the application of transverse load. This clearly shows that the non-composite assumption (where strands act independently) is not valid. Furthermore, the strands maintain the same level of stress at various distances from the anchorage (i.e., constant stress along the length of each strand).

The symmetric model of finite element analysis adopted in this paper can effectively model the tensile and bending behavior of the cable. Force changes due to axial and bending predicted using the FE models were in good agreement with the experimental results.

3.7 Reference for Chapter 3

Caballero, A. and Poser, M., 2010. Local bending stresses in stay cables with an elastic guide. Structural engineering international, 20(3), pp.254-259.

Engineering ToolBox, (2004). Friction - Friction Coefficients and Calculator. [online] Available at: https://www.engineeringtoolbox.com/friction-coefficients-d_778.html [Accessed 18.04.2023].

FIB Bulletins No. 89, 2019. FIB BULLETIN NO. 89, Title: Acceptance of stay cable systems using prestressing steels. The International Federation for structural concrete (FIB). https://www.fib-international.org/publications/fib-bulletins/acceptance-of-stay-cable-systems-using-prestressing-steels-pdf-detail.html

Fürst, A., Marti, P. and Ganz, H.R., 2001. Bending of stay cables. Structural Engineering International, 11(1), pp.42-46. https://doi.org/10.2749/101686601780324313

Li, P.J.; Wang, R.H.; Zhang, Y.; Qiu, B.; Zhou, X.R.; Ma, Y.; Tian, H. Precisely Identifying Method for Geometric Stiffness of Section of Cable Strut; Guangxi Transportation Research Institute: Nanning, China, 2012.

Nabizadeh, A., Al-Barqawi, M.O. and Tabatabai, H., 2021. Probabilistic Models for Fatigue Resistance of Seven-Wire Prestressing Strands and Stay Cables. Journal of Bridge Engineering, 26(10), p.04021070.

PCI design handbook: Precast and Prestressed Concrete. 8th edition,2017. https://www.pci.org/ItemDetail?iProductCode=MNL-120-17

Prato, C.A. and Ceballos, M.A., 2003. Dynamic bending stresses near the ends of parallel-bundle stay cables. Structural engineering international, 13(1), pp.64-68. https://doi.org/10.2749/101686603777965008

PTI DC-45, 2018. Recommendations for Stay Cable Design, Testing, and Installation (DC45.1-18), written by PTI Committee DC-45: Cable Stayed Bridge. https://www.post-tensioning.org/publications/store/productdetail.aspx?ItemID=DC451&Language=English&Units=US_Units

Shen, G., Macdonald, J. and Coules, H., 2022. Bending Fatigue Life Evaluation of Bridge Stay Cables. Journal of Engineering Mechanics, 148(3), p.04021168. https://doi.org/10.1061/(ASCE)EM.1943-7889.0002064

SPECIAL SPECIFICATION, 4604 Stay Cables, 2004, Texas Department of Transportation (TxDOT). https://ftp.dot.state.tx.us/pub/txdot-info/cmd/cserve/specs/2004/spec/ss4604.pdf

Winkler, J., Georgakis, C., Fischer, G., Wood, S. and Ghannoum, W., 2015. Structural response of a multi-strand stay cable to cyclic bending load. Structural Engineering International, 25(2), pp.141-150. https://doi.org/10.2749/101686614X14043795570138

Chapter 4: Simplified Design and Parametric Study of Bending Stress in Parallel Strand Stay Cables

4.1. Simplified design method

Experimental and FE results reported in Chapters 2 and 3 have established the fact that, contrary to a widely held view, the bending and axial stresses developed in strands as a result of the application of transverse loads on the stay cable are not a function of the apparent cable angle change alone. These stresses are also a function of the distance from the strand to the centroid of the strand group at the anchorages as well as the length of the cable. This paper summarizes the previous analysis results and puts forward a simplified design method for calculating the cable bending stress. Using the proposed design method, the maximum bending stresses in various sizes and lengths of stay cables are calculated as a result of the application of a single concentrated load at the mid-length of the cable.

Figure 4-1 shows a stay cable under the action of a concentrated load (P) at mid-length. Under the action of P, an apparent relative rotation angle α develops, with the resulting maximum displacement at cable mid-length of $\delta = \frac{\alpha L}{2}$ where L is the length of the cable.

In the transition zone (between anchor head and tension ring), the various strands in the cable are not in contact with each other except at the anchorage and the transition ring. This means that the strands within the transition zone deform independently (Figure 4-2). However, the rigid anchor head enforces compatibility at the end anchorage and does not allow relative slip. Figure 4-3 shows the geometric relationship in the transition zone after an angle change θ has occurred between the anchorage and deviation ring. Considering that the angle change θ/2 occurs at the anchorage (section 1) and the deviation ring (section 2), the change in length of

any strand s can be calculated. In stay cables where the deviation ring is unsupported, θ is expected to approach α. Therefore, for simplified calculations (conservatively), θ may be assumed to be equal to α.

The actual θ can be estimated using a finite difference model of the cable (described in Chapter 2), especially for cables with complicated loading and/or other spring supports along their length.

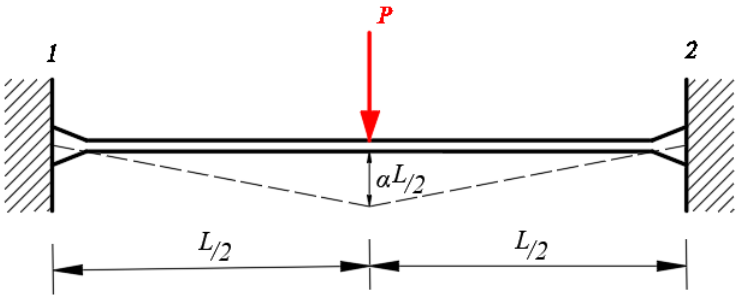

Figure 4-1. Sketch of a concentrated force at mid-length of a parallel strand stay cable.

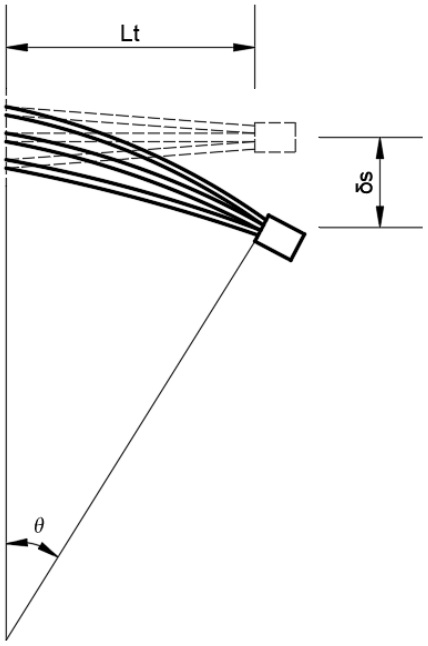

Figure 4-2. Strand deformation within the transition zone.

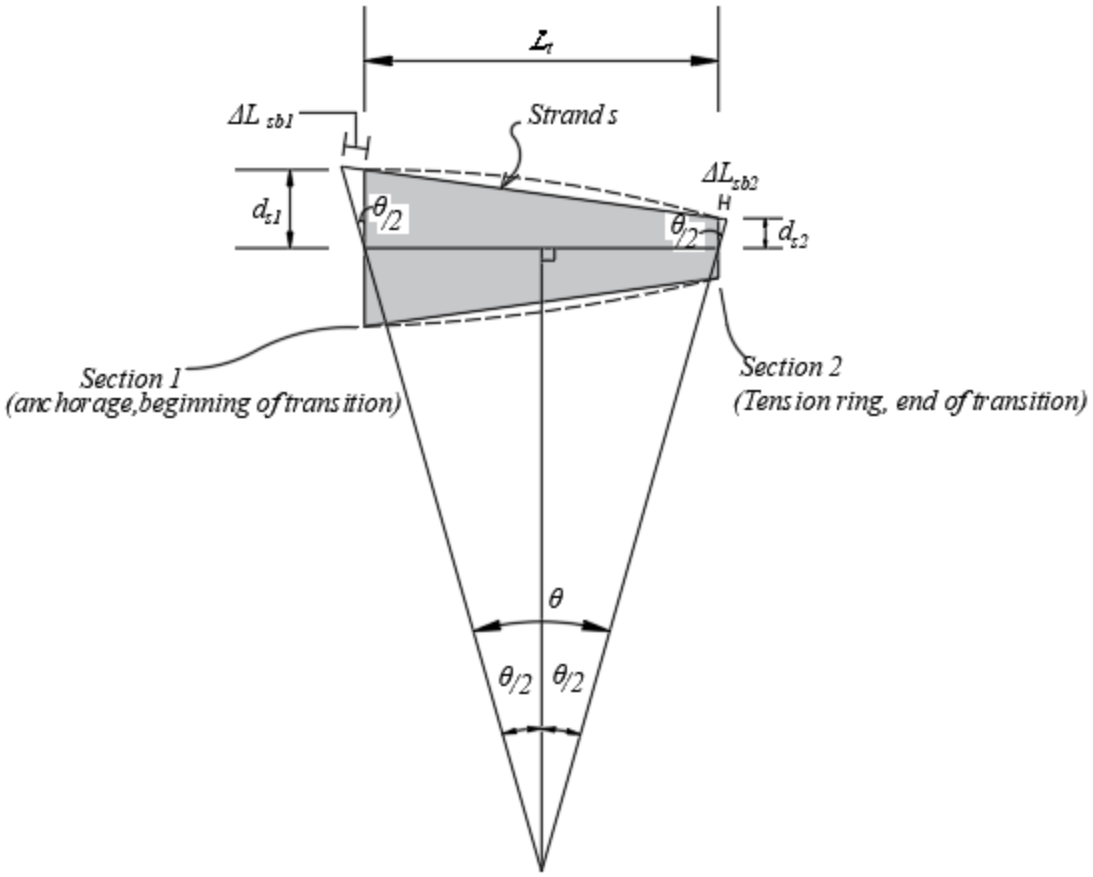

Figure 4-3. Geometric relationship of the transition zone of stay cables.

Change of length in strand $s = \Delta L_{sb}$

$$\Delta L_{sb} = \Delta L_{sb1} + \Delta L_{sb2} \quad (4\text{-}1)$$

$$\Delta L_{sb} = \frac{\theta}{2} d_{s1} + \frac{\theta}{2} d_{s2} = \theta\left(\frac{d_{s1}+d_{s2}}{2}\right) \quad (4\text{-}2)$$

ε_{sb}= bending strain in strand s due to bending action

$\Delta L_{sb1} =$ change of length of strand s at the section 1 (anchor head)

$\Delta L_{sb2} =$ change of length of strand s at the section 2 (tension ring)

$d_{s1} =$ distance between strand s and the centroid of the cable at section 1 (anchor head)$d_{s2} =$ distance between strand s and the centroid of the cable at section 2 (tension ring)

Since the common greased-and-sheathed strands used in stay cables are unbonded along their entire length, the sum of length changes of the strand at the two anchorages (one at each cable end) can be divided by the cable length L to calculate the strain due to bending action (ε_{sb}). Substituting for ΔL_{sb} from Equation 4-2:

$$\varepsilon_{sb} = \frac{2\Delta L_{sb}}{L} = \frac{\Delta L_{sb}}{L/2} = \frac{\theta(d_{s1}+d_{s2})}{L} \qquad (4\text{-}3)$$

Where α is the bending rotation angle, θ is the rotation angle within the transition zone, L is the cable length.

The application of transverse load P also generates an additional axial strain in the cable (ε_{sa}). The total strain (ε_s) is equal to the sum of the bending and axial components ($\varepsilon_{sb+}\varepsilon_{sa}$). ε_{sa}=is the axial strain in strand s due to bending action

For a cable with a transverse load applied at its mid-length, the axial strain due to cable deflection (ε_a) can be approximated as follows (Figure 4-1):

$$\varepsilon_a \cong \frac{2\sqrt{(l/2)^2+(\alpha L/2)^2}-L}{L} = \frac{L\sqrt{1+\alpha^2}-L}{L} = \sqrt{1-\alpha^2}-1 \qquad (4\text{-}4)$$

$$\varepsilon_s = \varepsilon_{sb+}\varepsilon_{sa} = \frac{\theta(d_{s1}+d_{s2})}{L} + \sqrt{1+\alpha^2}-1 \qquad (4\text{-}5)$$

If the angle change within the transition zone (θ) is equal to α

$$\varepsilon_s = \frac{\alpha(d_{s1}+d_{s2})}{L} + \sqrt{1+\alpha^2}-1 \qquad (4\text{-}6)$$

The estimated bending stress (σ_s) can then be calculated by multiplying by the modulus of elasticity of the strand (E = 28,500 ksi).

$$\sigma_s = E\varepsilon_s \qquad (4\text{-}7)$$

The above equations (4-6 and 4-7) are proposed as simple equations to calculate bending stresses in cables subjected to transverse loads on the cable. For more complex

transverse loads (such as distributed and/or concentrated loads, Figure 4-4) and when neoprene washers are used in the guide pipe, a similar approach can be followed using finite difference modeling. For a general transverse loading case, the finite difference approach can be utilized to calculate θ (angle change within the transition zone). The general finite difference formulation proposed by Mehrabi and Tabatabai (1998) can incorporate spring support for the cable. Neoprene washers can be modeled as springs in the finite difference model. Also, ε_a can be estimated by integrating measured nodal deflections from the finite difference analysis.

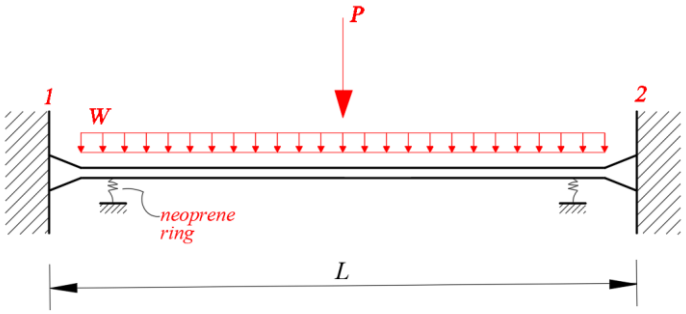

Figure 4-4. A parallel strand stay cable with different transverse forces and neoprene rings.

When the rotation angle is 0.025 rad, the strand stresses (from the 5-strand stay cable test described in Chapter 3) as well as the corresponding stresses obtained from the FE results and the proposed simplified procedures (Equations 4-6 and 4-7) can be plotted as shown in Figure 4-5. The results from the simplified procedure are in good agreement with the FE results (top: 19.5 ksi, core: 8.9 ksi, bottom: -1.24 ksi).

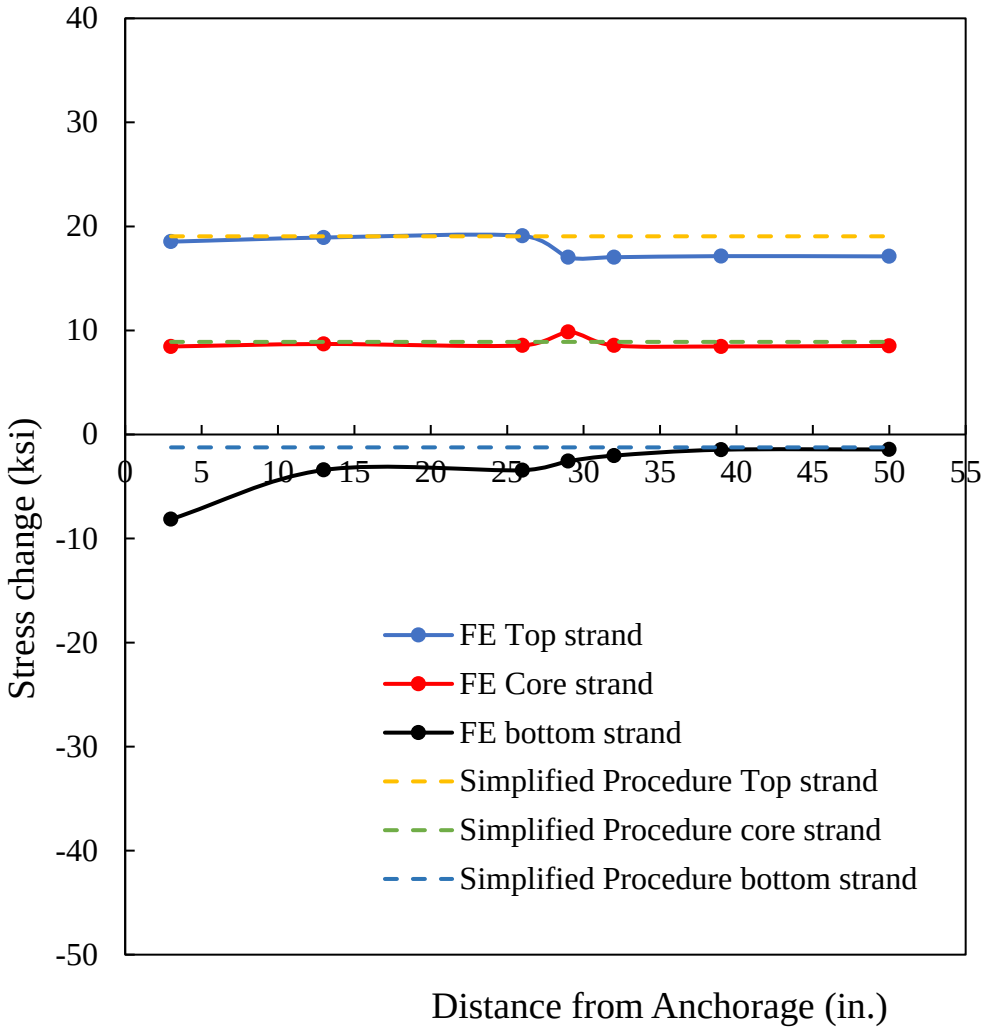

Figure 4-5. Bending stresses in the top, center, and bottom strands of the 5-strand cable (at a rotation angle of 0.025 rad)

The following example illustrates the calculation process for estimating bending stresses due to the application of a transverse force at the mid-length of a stay cable.

4.2. Example

A 19-strand stay cable is subjected to a concentrated force at mid-length. The cross sections at both ends of the transition zone are shown in Figure 4-7 (a,b). The imposed rotation due to

the concentrated load is assumed to be 0.025 radians (consistent with the maximum rotation angle in the PTI and fib standards). The length of the cable is 50 ft. Estimate the maximum bending stress due to the application of transverse load.

Solution:

L = 50ft. = 600 in., $\alpha = 0.025\ rad$.

Figure 4-3 shows the distances from the strand located farthest from the center of the 19-strand cable at the anchorage and deviation ring: d_{s1} =2.757 in., d_{s2} =1.362 in.

Therefore, using Equation 4-6:

$$\varepsilon_s = \frac{\alpha(d_{s1} + d_{s2})}{L} + \sqrt{1 + \alpha^2} - 1 = \frac{0.025(2.757 + 1.36)}{600} + \sqrt{1 + 0.025^2} - 1$$

$$\varepsilon_s = 0.004841$$

$$\sigma_{s\cdot max} = E\varepsilon_s = 28500ksi \times 0.0004841 = 13.80ksi$$

4.3. Parametric study

Table 4-1 provides the calculated maximum bending stresses for 5-, 19-, 48-, and 85-strand stay cables with various cable lengths of 15, 50, 100, 200, and 400 ft. The bending stresses are calculated for α equal to 0.01 and 0.025 radians. The cross sections of various size cables are shown in Figure 4-6. The patterns of 19, 48, and 85 strand stay cables are obtained from real projects.

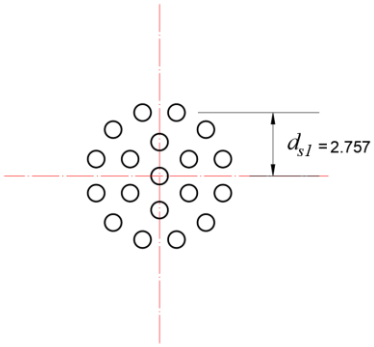

(a) Anchorage end of 19-strands

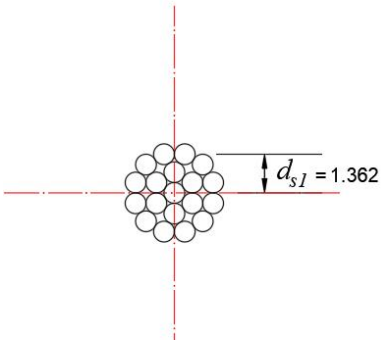

（b） Tension ring end of 19-strands

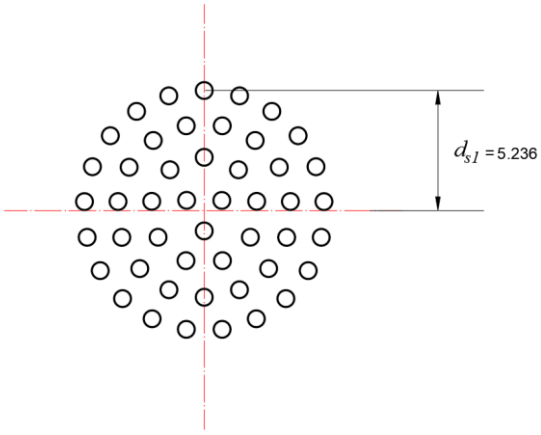

(c) Anchorage end of 48-strands

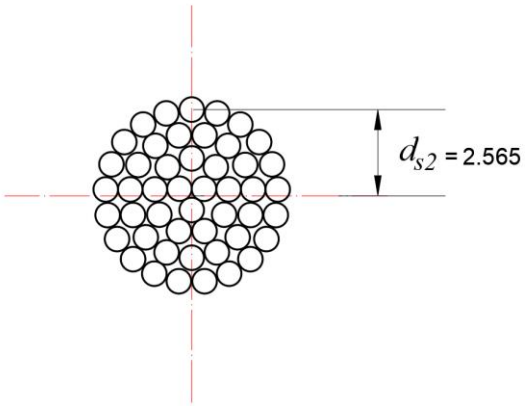

（d） Tension ring end of 48-strands

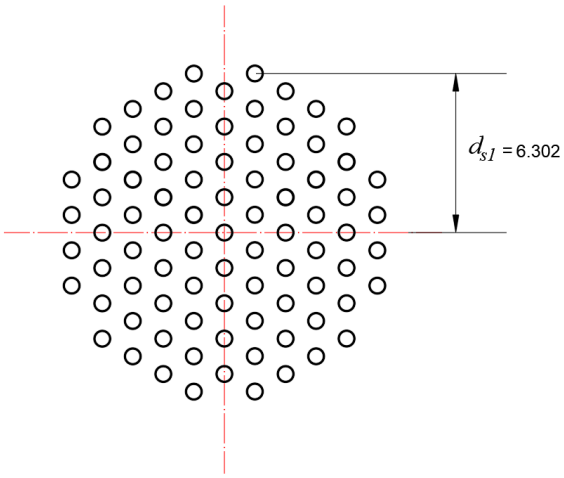

(e) Anchorage end of 85-strands

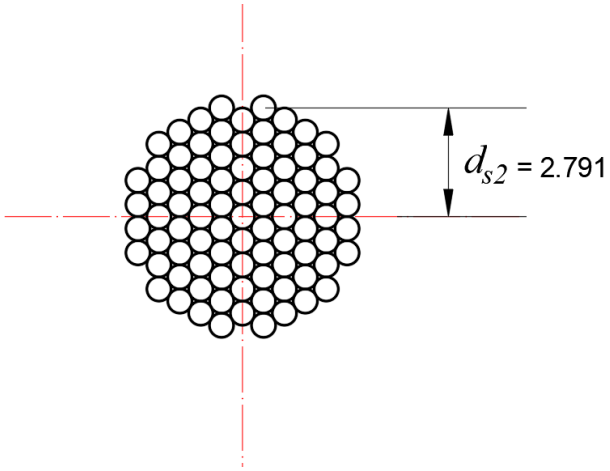

（f） Tension ring end of 85-strands

Figure 4-6. Cross-sections at both ends of the transition zone (in inches)

The maximum bending stress of the same stay cable decreases as the length increases, which is consistent with the calculation Equation (4-6). As the cable length increases, the strain generated by the change in length at the ends of the transition zone becomes smaller. Furthermore, as the cable size increases, the bending stresses increase for a given L and a. The cable with a 15-ft length shown in Table 4-1 is not a typical stay cable. However, this length is analyzed because the fib Bulletin 89 standard (reference) specifies a stay cable bending qualification test that is based on a short cable. In the fib standard, 0.01 and 0.025-radian angle changes are imposed regardless of the size of the cable used. The fib standard implies that the only relevant parameter is the angle change. However, results in Table 4-1 indicate that bending stresses are not a function of angle alone. They are also a function of cable size and length.

Table 4-1 Maximum bending stress in stay cables with various cable sizes and lengths

Strands	ds1 (in.)	ds2 (in.)	Length (ft.)	Max. bending stress (ksi)	α (rad)
5	2.09	0.53	15*	5.57	0.01
			50	2.67	
			100	2.05	
			200	1.73	
			400	1.58	
19	2.757	1.362	15*	7.95	
			50	3.38	
			100	2.40	
			200	1.91	
			400	1.67	
48	5.236	2.565	15*	13.78	
			50	5.13	
			100	3.28	
			200	2.35	
			400	1.89	
85	6.302	2.791	15*	15.82	
			50	5.74	
			100	3.58	
			200	2.50	
			400	1.96	

* 15 ft. length is the minimum fib length for tests.

Table 4-1 Maximum bending stress in stay cables with various cable sizes and lengths. (Continued)

Strands	ds1 (in.)	ds2 (in.)	Length (ft.)	Max. bending stress (ksi)	α (rad)
5	2.09	0.53	15*	19.27	0.025
			50	12.02	
			100	10.46	
			200	9.68	
			400	9.29	
19	2.757	1.362	15*	25.21	
			50	13.80	
			100	11.35	
			200	10.13	
			400	9.52	
48	5.236	2.565	15*	39.78	
			50	18.17	
			100	13.54	
			200	11.22	
			400	10.06	
85	6.50	3.10	15*	44.90	
			50	19.70	
			100	14.30	
			200	11.60	
			400	10.25	

4.4. Conclusions

A simplified calculation method for determining the bending stresses in strands of a parallel strand stay cable subjected to transverse loads is presented (Equations 4-6 and 4-7). The bending strains (and stresses) of each strand can be calculated using Equation 6, which is a function of the apparent rotation angle (a), size (diameter) of cable, and cable length.

It is important to emphasize that the bending stress in cables is not related to the rotation angle alone, contrary to widely held belief by designers and design standards (PTI DC-45 and fib Bulletin 89).

The parametric study shows that, as the length increases, the strain generated by the strand position at the expansion end of the transition zone becomes smaller, so related bending stress is reduced.

4.5. References for Chapter 4

Mehrabi, A.B. and Tabatabai, H., 1998. Unified finite difference formulation for free vibration of cables. Journal of Structural Engineering, 124(11), pp.1313-1322.

PTI DC-45, 2018. Recommendations for Stay Cable Design, Testing, and Installation (DC45.1-18), written by PTI Committee DC-45: Cable Stayed Bridge.

FIB Bulletins No. 89, 2019. FIB BULLETIN NO. 89, Title: Acceptance of stay cable systems using prestressing steels. The International Federation for structural concrete (FIB). https://www.fib-international.org/publications/fib-bulletins/acceptance-of-stay-cable-systems-using-prestressing-steels-pdf-detail.html

Chapter 5: Summary and Conclusions

Stay cables are the most critical components of cable-stayed bridges. Besides axial tension, the parallel strand stay cables are also subjected to bending stresses due to wind, vibrations, and load-induced rotations of the superstructure and towers at cable ends.

Traditionally, designers have assumed that the strands form a non-composite bundle (non-composite moments of inertia) due to a lack of sufficient bond between strands along the length of the cable. Most modern stay cables consist of greased-and-sheathed 7-wire strands. Therefore, composite, or partially composite effects are generally not considered. This assumption ignores the fact that relative slippage between strands (which is needed for non-composite action) cannot occur since the anchorage plates do not allow relative slip between strands (i.e., compatibility of strains is enforced at the cable ends even though the strands are not in contact with each other in the transition zone). Also, periodic cable bands (banding the strands together) along the free length of the cable may provide a degree of composite action. The governing design standard for parallel strand stay cables in the U.S. (PTI DC-45) as well as industry practice considers the apparent angular rotation as the only parameter influencing bending stresses in stay cables. The stay cable bending qualification fatigue test specified in fib Bulletin No. 89 involves imposing angle changes of 0.01 and 0.025 radians regardless of the cable size and length. This implies that cable size and length do not influence bending stresses in stay cables.

This study examines the extent of composite action between stay cable strands due to applied transverse loads through experimental and computational models. The development of bending stresses in various strands within the transition zone (due to the application of

transverse forces on the cable) is evaluated. Simplified calculation procedures for bending stresses are proposed. The computational models and the calculation procedures are verified using the results of laboratory experiments performed on single strand and 5-strand cables. An approach based on a finite difference model is also discussed. The finite difference approach can help determine angular changes and deflection profile under any transverse loading condition, which can then be used to estimate rotation angles and bending stresses using the simplified calculation procedures.

Based on experimental and analytical studies, the following conclusions are made:

1. Although individual 7-wire strands within the transition zone of stay cables (near anchorages) are not in contact with each other, the assumption of fully non-composite behavior does not explain the response observed in physical tests and finite element models.

2. The bending stress generated in each stay cable strand is proportional to the average vertical distance from the center of that strand to the centroid of the cable at the anchorage and the deviation ring ($\frac{d_{s1}+d_{s2}}{2}$). The bending stress is also proportional to the apparent rotation angle within the transition zone (θ) and is inversely proportional to the cable length (L). Therefore, the assumption commonly made that rotation angle alone can represent the bending stresses in a stay cable is not valid.

3. Results of experimental and computational models show that strand stress increments developed due to the application of transverse loads on the cable are constant along the length of each strand. The stress increments are at their highest and lowest levels in top and bottom strands, respectively. The stress increments in the center (core) strand are equal to the axial strain change resulting from cable length change due to deformation under load.

4. In-plane bending moments developed in the cable at the anchorage plate (M1) and the deviation ring (M2) are equal to the sum of each strand's force (which is constant along its length) times the vertical distance to the centroid of the cable cross section at each location.

5. Experimental results indicate that an equivalent solid cylindrical finite element model of the strand (with partially restrained boundary conditions) can accurately represent the behavior of the 7-wire strand. The equivalent cylindrical model can then be used to model multi-strand cables with reduced computational time (compared to modeling all wires individually). A 5-strand finite element model using this approach properly represented the experimental results. To introduce initial tension (pretension) in the cable model before application of transverse load, a fictitious temperature change was applied to the cable model.

6. Simplified calculation procedures are proposed to estimate bending stresses in each strand of a multi-strand stay cable due to the application of transverse loads on the cable. The bending stress is proportional to the angle change due to loading and average eccentricity of the strand at the anchorage zone and deviation ring and is inversely proportional to cable length. The axial stress change due to cable bending can be estimated from an idealized deflection profile in a cable subjected to one or more concentrated loads.

7. The finite difference method proposed by Mehrabi and Tabatabai (1998) can be used to calculate the displacement profile and angle change within the transition zone in cases where complicated loading and/or neoprene washers (idealized springs) is considered. Finite difference results can then be used in the simplified calculation procedures to estimate bending stresses.

8. Parametric studies performed using the developed simplified procedures indicate that bending stresses due to angle changes of 0.01 or 0.025 radians can be substantially higher in large and short cables. The fib Bulletin 89 (fib 2019) bending fatigue test procedures should be modified to consider the cable size and length parameters.

Recommendations for Future Research

This research addressed bending stresses developed due to transverse loads applied along the length of a stay cable. Future works should address bending stresses imposed on the cable through the rotation of cable ends due to the effects of loads on the superstructure and the towers. Furthermore, the effect of cable inclination, dynamic loading, cable bands, and dampers should be studied. The developed simplified calculation procedures can also be applied to the calculation of stress in unbonded tendons of post-tensioned beams.